Vol. 47 — N° 1 03 23 p. 23 – 48

GEOSTANDARDS and GEOANALYTICAL RESEARCH

Testing Nano-Powder and Fused-Glass Mineral Reference Materials for *In Situ* Rb-Sr Dating of Glauconite, Phlogopite, Biotite and Feldspar via LA-ICP-MS/MS

Ahmad **Redaa** (1, 2)*, Juraj **Farkaš** (1, 3), Sarah **Gilbert** (4), Alan S. **Collins** (1, 3), Stefan **Löhr** (1, 5), Davood **Vasegh** (6), Marnie **Forster** (3, 6), Morgan **Blades** (1, 3), Thomas **Zack** (1, 7), Andrea **Giuliani** (8), Roland **Maas** (9), Andre **Baldermann** (10), Martin **Dietzel** (10) and Dieter **Garbe-Schönberg** (11, 12)

(1) Department of Earth Sciences, Metal Isotope Group (MIG), University of Adelaide, Adelaide, Australia
(2) Faculty of Earth Sciences, King Abdulaziz University, Jeddah, Saudi Arabia
(3) MinEx Cooperative Research Centre (CRC), University of Adelaide, Adelaide, Australia
(4) Adelaide Microscopy, University of Adelaide, Adelaide, Australia
(5) School of Natural Sciences, Macquarie University, Sydney, Australia
(6) Research School of Earth Sciences, Australian National University, Canberra, Australia
(7) Department of Earth Sciences, University of Gothenburg, Gothenburg, Sweden
(8) Institute of Geochemistry and Petrology, Department of Earth Sciences, Zürich, ETH, Switzerland
(9) School of Earth Sciences, Faculty of Science, University of Melbourne, Australia
(10) Institute of Applied Geosciences, Graz University of Technology and NAWI Graz Geocentre, Graz, Austria
(11) Institute of Geosciences, Kiel University, Kiel, Germany
(12) Department of Physics and Earth Sciences, Jacobs University, Bremen, Germany
* Corresponding author. e-mail: ahmad.redaa@adelaide.edu.au, areda@kau.edu.sa

Reference materials (RMs) with well-characterised composition are necessary for reliable quantification and quality control of isotopic analyses of geological samples. For *in situ* Rb-Sr analysis of silicate minerals via laser ablation inductively coupled plasma tandem mass spectrometry (LA-ICP-MS/MS) with a collision/reaction cell, there is a general lack of mineral-specific and matrix-matched RMs, which limits wider application of this new laser-based dating technique to certain minerals. In this work, pressed nano-powder pellets (NP) of four RMs, GL-O (glauconite), Mica-Mg (phlogopite), Mica-Fe (biotite) and FK-N (K-feldspar), were analysed and tested for *in situ* Rb-Sr dating, complemented by isotope dilution (ID) MC-ICP-MS Rb-Sr analyses of GL-O and Mica-Mg. In addition, we attempted to develop alternative flux-free and fused 'mineral glasses' from the above RMs for *in situ* Rb-Sr dating applications. Overall, the results of this study showed that among the above RMs only two NP (Mica-Mg-NP and GL-O-NP) were suitable and robust for *in situ* dating applications. These two nano-powder reference materials, Mica-Mg-NP and GL-O-NP, were thus used as primary RMs to normalise and determine Rb-Sr ages for three natural minerals: MDC phlogopite and GL-O glauconite grains, and also Mica-Fe-NP (biotite). Our *in situ* analyses of the above RMs yielded Rb-Sr ages that are in good agreement (within 8%) of published ages, which suggests that both Mica-Mg-NP and GL-O-NP are suitable RMs for *in situ* Rb-Sr dating of phlogopite, glauconite and biotite. However, using secondary RMs is recommended to monitor the quality of the obtained ages.

Keywords: *in situ* Rb-Sr dating, LA-ICP-MS/MS, reference materials, nano-powders.

Received 29 Dec 21 – Accepted 26 Sep 22

In situ Rb-Sr dating of silicate minerals and rocks using laser ablation-inductively coupled plasma tandem mass spectrometry with a collision/reaction cell (LA-ICP-MS/MS) is becoming an increasingly popular geochronological technique to constrain the timing of mineral formation, cooling/resetting ages as well as the duration of geological events (Hogmalm *et al.* 2017, Tillberg *et al.* 2017, 2020, Li *et al.* 2020, Olierook *et al.* 2020, Redaa *et al.* 2021, Redaa

doi: 10.1111/ggr.12467

et al. 2022). This novel and rapid dating technique allows for interference-free measurement of isobaric ^{87}Rb and ^{87}Sr isotopes in K- and Rb-rich minerals such as glauconite, illite, micas and K-feldspar. *In situ* Rb-Sr dating is facilitated by a collision/reaction cell between two quadrupole mass filters (MS/MS system) with either N_2O or SF_6 reaction gases, which allows chemical separation of Sr from Rb, as the latter does not react with either of these gases (Hogmalm *et al.* 2017, Bevan *et al.* 2021). Rubidium can be measured by monitoring ^{85}Rb counts per second (cps) as the proxy for ^{87}Rb where ^{87}Rb = ^{85}Rb × 0.38562 (Rosman and Taylor 1999), while the reactive Sr isotopes can be measured interference-free as 'mass-shifted' Sr species (e.g., $^{87}Sr^{16}O^+$ or $^{87}Sr^{19}F^+$ at masses 103 or 106 amu, respectively). Another advantage of the *in situ* Rb-Sr dating method is that these measurements can be done rapidly and relatively precisely (depending on whether single or multi-collector LA-ICP-MS/MS instruments are employed) with minimal sample preparation, as the mineral of interest can be analysed directly from rock chips as polished-mounts or polished-thick-sections (ideally > 50 μm thick), without the need for time-consuming mineral and chemical separation that is conventionally required to remove the isobaric interference between ^{87}Rb and ^{87}Sr (see Pin and Bassin 1992). In addition, contamination by other phases in the mineral of interest (from inclusions or overgrowths) can be avoided at the micro-scale as the typical LA spot size for Rb-Sr dating is on the order of 50–80 μm (Zack and Hogmalm 2016, Hogmalm *et al.* 2017, Redaa *et al.* 2021). However, the robustness and repeatability of *in situ* Rb-Sr dating of silicate minerals is currently restricted by several factors including elemental fractionation effects (Gilbert *et al.* 2014, Lin *et al.* 2016, Zhang *et al.* 2016) and mineral specific ablation properties of reference materials (RMs) and samples of interest (i.e., matrix effects) (Sylvester 2008, Agatemor and Beauchemin 2011, Redaa *et al.* 2021).

The above factors can be eliminated or minimised by the application of suitably matrix-matched RMs combined with calibration and data correction routines summarised in Miliszkiewicz *et al.* (2015) and references therein. However, the general lack of well-characterised and matrix-matched RMs for *in situ* Rb-Sr measurement remains one of the main challenges for this dating technique as only a limited number of suitable RMs are available to calibrate *in situ* ^{87}Rb/^{86}Sr and ^{87}Sr/^{86}Sr data. Specifically, most recent *in situ* Rb-Sr dating studies have relied on a combination of the following RMs, including: the glasses NIST SRM 610, BCR-2G and BHVO-2G, and a single available nano-powder (NP) phlogopite RM (Mica-Mg-NP) (Table 1) (Zack and Hogmalm 2016, Hogmalm *et al.* 2017, Şengün *et al.* 2019, Armistead *et al.* 2020, Gorojovsky and Alard 2020, Li *et al.* 2020, Olierook *et al.* 2020, Tillberg *et al.* 2020, Laureijs *et al.* 2021, Redaa *et al.* 2021). In addition, some MPI-DING glasses were used as RMs for *in situ* dating, including ATHO-G (rhyolite), T1-G (quartz-diorite) and StHs6/80-G (andesite) (Laureijs *et al.* 2021), and their ^{87}Sr/^{86}Sr recommended values are listed in Table 1.

The ^{87}Rb/^{86}Sr ratios of the above materials have been constrained and derived either from (i) Rb and Sr mass fractions in the total sample mass, and/or (ii) calculated indirectly from measured ^{87}Sr/^{86}Sr (via LA-ICP-MS/MS, TIMS, MC-ICP-MS) and published 'age' data (i.e., available crystallisation age and an assumed initial Sr isotope composition following the approach of Hogmalm *et al.* (2017)). In addition, the ^{87}Rb/^{86}Sr ratio of Mica-Mg was directly measured using an ID MC-ICP-MS method (Jegal *et al.* 2022). To date a range of accepted ^{87}Rb/^{86}Sr and ^{87}Sr/^{86}Sr ratios and ages for the above RMs have been reported in the literature (see data in Table 1), and these ratios can be used as working values to calibrate Rb-Sr data obtained via LA-ICP-MS/MS. However, using the above RMs, such as NIST SRM 610 as illustrated by Redaa *et al.* (2021), for *in situ* Rb-Sr dating of natural minerals could bias the accuracy of *in situ* Rb-Sr ages by up to 7% (tested on natural phlogopite crystals). This is mostly due to differences in the chemical and physical (i.e., ablation) properties of RMs and mineral(s) of interest.

The current approach for *in situ* Rb-Sr dating, designed to overcome these matrix effects, relies primarily on the analysis of additional RMs (i.e., well-characterised natural minerals) with previously determined ages which can be used to monitor the overall quality and repeatability of *in situ* Rb-Sr data (Armistead *et al.* 2020, Li *et al.* 2020, Olierook *et al.* 2020, Bevan *et al.* 2021, Laureijs *et al.* 2021, Redaa *et al.* 2021). Such monitoring of data quality, along with the application of secondary calibration when needed, allows *in situ* Rb-Sr ages to be determined with an accuracy and precision ranging between 1.5% to 3% (Armistead *et al.* 2020, Li *et al.* 2020, Olierook *et al.* 2020, Bevan *et al.* 2021, Redaa *et al.* 2021, Subarkah *et al.* 2021). These values are however above typical uncertainties achievable with solution based single-collector instruments, which calls for the development and testing of new mineral-specific reference materials to further improve the accuracy and robustness of *in situ* Rb-Sr dating of silicate minerals. Such new mineral-specific RMs need to be isotopically homogeneous at the micro-scale, and can be either crystalline minerals or produced in the form of (i) pressed powder pellets with binders (O'Connor *et al.* 2007, Tabersky *et al.* 2014), (ii) pressed NP pellets without binders

Table 1.
Reported $^{87}Rb/^{86}Sr$ and $^{87}Sr/^{86}Sr$ ratios of reference materials used in previous studies focusing on *in situ* Rb-Sr dating via LA-ICP-MS/MS (see References)

Reference material	Type	$^{87}Rb/^{86}Sr \pm 2s$	$^{87}Sr/^{86}Sr \pm 2s$	References
NIST SRM 610	Glass	2.33 ± 0.0049	0.709699 ± 0.000018*	(Hogmalm *et al.* 2017)
		2.3894 ± 0.8	0.709699 ± 0.000018*	(Bevan *et al.* 2021)
		2.390 ± 0.005	0.709699 ± 0.000018*	(Olierook *et al.* 2020)
BCR-2G	Glass	0.3901	0.705003	(Elburg *et al.* 2005, Hogmalm *et al.* 2017)
USGS BHVO-2G	Glass	0.06557 ± 0.00066	0.703469 ± 0.000007	(Elburg *et al.* 2005, Gorojovsky and Alard 2020)
ATHO-G	Glass	-	0.703224	(Jochum *et al.* 2006, Laureijs *et al.* 2021)
T1-G	Glass	-	0.710093 ± 0.000004	(Jochum *et al.* 2006, Laureijs *et al.* 2021)
StHs6/80-G	Glass	-	0.703497 ± 0.000008	(Jochum *et al.* 2006, Laureijs *et al.* 2021)
Mica-Mg-NP	Pressed nano-powder pellet of phlogopite	154.6 ± 1.93	1.8525 ± 0.0024	(Hogmalm *et al.* 2017)
		156.9 ± 2.3	1.8692 ± 0.0022	(Olierook *et al.* 2020)
		155.6 ± 7.3	1.8622 ± 0.0067	(Jegal *et al.* 2022)
		155.27 ± 2.0**	1.857 ± 0.013	This study (LA-ICP-MS/MS)
		151.4 ± 0.54	1.8406 ± 0.0002	This study (MC-ICP/MS)
GL-O-NP	Pressed nano-powder pellet of glauconite	-	0.7535 ± 0.0010	(Govindaraju 1995)
		36.2 ± 4.0	0.75305 ± 0.00089	(Jegal *et al.* 2022)
		35.46 ± 0.88**	0.7547 ± 0.0031	This study (LA-ICP-MS/MS)
		36.57 ± 0.26	0.753561 ± 0.00032	This study (MC-ICP/MS)

* This value is originally reported in Woodhead and Hergt (2001).
** calculated $^{87}Rb/^{86}Sr$ ratios based on assumed ages of 519.4 ± 6.5 Ma and 95.4 Ma for Mica-Mg and GL-O respectively.

(Garbe-Schönberg and Müller 2014), or (iii) fused mineral glasses with a flux (Eggins 2003, Yu *et al.* 2003, Awaji *et al.* 2006) or (iv) flux-free glasses (Fedorowich *et al.* 1993, He *et al.* 2016).

In this study, four mineral RMs including phlogopite (Mica-Mg-NP), glauconite (GL-O-NP), biotite (Mica-Fe-NP), and K-feldspar (FK-N-NP) – available via Centre de Recherches Pétrographiques et Géochimiques (CRPG) – were prepared as pressed NPs, and analysed by LA-ICP-MS/MS for $^{87}Rb/^{86}Sr$ and $^{87}Sr/^{86}Sr$ isotopic compositions. The original powders Mica-Mg and GL-O were also analysed by isotope dilution (ID) MC-ICP-MS. Furthermore, we also attempted to develop and produce a set of flux-free mineral glasses. These NPs and fused glasses were assessed for their elemental and isotopic composition and homogeneity, and their suitability for *in situ* Rb-Sr dating of K-rich silicate minerals via LA-ICP-MS/MS.

Samples and analysed materials

GL-O glauconite

GL-O consists of glauconite grains, an Fe- and K-rich mica group mineral, $(K,Na)(Fe^{3+},Al,Mg)_2(Si,Al)_4O_{10}(OH)_2$, sampled from the *Mantelliceras mantellii* ammonite zone near the beach of Cauville from the basal Cenomanian section at Pays de Caux, Normandy, France (Govindaraju 1994). This RM is distributed by the CRPG as either grains or powders. The GL-O grains were assumed to be mineralogically homogeneous, but a recent study by Boulesteix *et al.* (2020), as well as Jegal *et al.* (2022) and our own investigations, show that some of the GL-O glauconite grains are inhomogeneous with complex textures, containing minor apatite and calcite inclusions and/or rims. GL-O was investigated in detail as a RM for K-Ar and Rb-Sr dating by Odin *et al.* (1982), and the mean K-Ar age of the 'bulk' sample is reported at 95 ± 1 Ma (see also Smith *et al.* 1998, Fiet *et al.* 2006, Derkowski *et al.* 2009), the latter also confirmed by a new *in situ* K-Ar technique that yielded 94 ± 1 Ma (Solé 2021). However, GL-O powders and grains investigated in Odin *et al.* (1982) yielded Rb-Sr ages that are highly variable with a mean of 91.7 ± 7.1 Ma (2*s*, *n* = 20) recalculated from Odin *et al.* (1982) using the revised ^{87}Rb decay constant of $1.3972 \pm 0.0045 \times 10^{-11}$ (Villa *et al.* 2015) and the expected Sr isotope composition of seawater at 95–100 Ma (0.70740 ± 0.0001) (see Veizer *et al.* 1999, McArthur *et al.* 2012 and references therein). Such differences in Rb-Sr ages of GL-O were attributed to the analytical procedures used and/or possible heterogeneity of the GL-O samples (Odin *et al.* 1982, Jegal *et al.* 2022). Based on later studies and K-Ar dating, GL-O was used to determine the age of the

Albian–Cenomanian boundary at 95 Ma (Fiet *et al.* 2006). However, Selby (2009) argued that this age (95 Ma) is younger than the depositional age of the *Mantelliceras mantellii* ammonite zone, where GL-O was sourced, which was constrained via U-Pb dating at 99.6 ± 0.9 Ma. Therefore, the glauconite probably formed or 'matured' within a period of 4–5 Ma after the deposition of the sediment, or alternatively it was formed at 99–100 Ma but the K-Ar (and by inference also Rb-Sr) system did not close until about 95 Ma. Accordingly, the mean GL-O age can be calculated at 95.4 ± 2.3 Ma (1SE) based on the above Rb-Sr, K-Ar and U-Pb depositional ages. The reported $^{87}Sr/^{86}Sr$ values of the 'bulk' GL-O material are 0.7535 ± 0.0010 (Govindaraju 1995), and 0.75305 ± 0.00089 (Jegal *et al.* 2022), and 36.2 ± 4.0 for $^{87}Rb/^{86}Sr$ (Jegal *et al.* 2022) (see Table 1).

Mica-Mg phlogopite

Phlogopite ($K(Fe,Mg)_3(AlSi_3O_{10})(OH)_2$) is the Mg member of the annite-phlogopite series. The Mica-Mg phlogopite was sampled and separated from a pegmatitic unit from the Ampandrandava quarry in the Bekily region, Madagascar (Govindaraju 1979, Govindaraju 1994), and it is distributed by the CRPG. This RM contains high Rb (1300 ± 40 μg g^{-1}) and low Sr (27 ± 3 μg g^{-1}) contents (Govindaraju 1979, Govindaraju 1994). The age of Mica-Mg has been constrained from various samples from the Bekily area by different geochronological methods including Rb-Sr, K-Ar and U-Pb dating. The mean crystallisation age of the Mica-Mg phlogopite is estimated at 519.4 ± 6.5 Ma with an initial $^{87}Sr/^{86}Sr$ of 0.72607 ± 0.0007 constrained from a diopside (low-Rb mineral) that occurs in the same location as Mica-Mg phlogopite (see Hogmalm *et al.* 2017 and references therein). The recommended $^{87}Rb/^{87}Sr$ and $^{87}Sr/^{86}Sr$ ratios of Mica-Mg reported in the literature are variable, i.e., Hogmalm *et al.* (2017) reported $^{87}Rb/^{87}Sr$ and $^{87}Sr/^{86}Sr$ ratios for Mica-Mg of 154.6 ± 1.93 and 1.8525 ± 0.0024, respectively; whereas Olierook *et al.* (2020) reported ratios of 156.9 ± 2.3 and 1.8692 ± 0.0022, respectively (Table 1). These $^{87}Sr/^{86}Sr$ values were measured by LA-ICP-MS/MS and $^{87}Rb/^{87}Sr$ was calculated by assuming the age of Mica-Mg is 519.4 ± 6.5 Ma with an initial $^{87}Sr/^{86}Sr$ of 0.72607 ± 0.0007 as described in Hogmalm *et al.* (2017). A recent study reported $^{87}Rb/^{87}Sr$ and $^{87}Sr/^{86}Sr$ ratios of 155.6 ± 7.3 and 1.8622 ± 0.0067, respectively with a calculated age of 521 ± 24 Ma, constrained by ID-TIMS and MC-ICP-MS (Jegal *et al.* 2022). In addition, novel *in situ* K-Ar dating of Mica-Mg yielded an age of 525 ± 10 Ma (Solé 2021). The variations in the reported absolute ratios suggest some heterogeneity between batches and/or between pressed NP pellets, however, the age is likely to be homogeneous. Therefore, it is recommended that for each Mica-Mg-NP pellet used for LA-ICP-MS/MS the $^{87}Rb/^{87}Sr$ should be characterised via measuring the $^{87}Sr/^{86}Sr$ and assuming an age and initial Sr ratio as described above (Hogmalm *et al.* 2017, Olierook *et al.* 2020).

MDC phlogopite

MDC phlogopite was acquired from the same area as Mica-Mg near Bekily, Madagascar (see Redaa *et al.* 2021) and has an expected age of 519.4 ± 6.5 Ma (Hogmalm *et al.* 2017). Thick flakes of this sample were vertically mounted in epoxy resin and polished. MDC was analysed in this work as an unknown sample.

Mica-Fe biotite

Mica-Fe is a biotite ($K(Fe,Mg)_3(AlSi_3O_{10})(OH)_2$) mica which was sampled from Massif de Saint-Sylvestre, France (Govindaraju 1979), and it is distributed by the CRPG. Mica-Fe has high Rb (2200 ± 2 μg g^{-1}) but low Sr (5 ± 1 μg g^{-1}) contents (Govindaraju 1979, Govindaraju 1994). Its reported K-Ar and Ar-Ar ages are 316 ± 9 Ma (Zimmermann *et al.* 1985) and 307.6 ± 0.4 Ma (Grove and Harrison 1996), respectively. Govindaraju (1979) also proposed Rb-Sr and K-Ar ages of 316 ± 10 Ma and 310 ± 10 Ma, respectively, and more recently Jegal *et al.* (2022), reported a Rb-Sr age of 287 ± 55 Ma. The initial $^{87}Sr/^{86}Sr$ ratio for Mica-Fe has not yet been measured directly, but it can be inferred from the Rb-Sr system of the coeval Saint-Sylvestre granite, which has a reported initial $^{87}Sr/^{86}Sr$ ratio of 0.709797 ± 0.016 (Turpin *et al.* 1990).

FK-N K-feldspar

FK-N is a K-rich alkali feldspar (i.e., microcline $KAlSi_3O_8$), which was sourced from the Madras area in India, and it is distributed by the CRPG. This RM contains 860 ± 56 μg g^{-1} of Rb and 39 ± 9 μg g^{-1} of Sr (Govindaraju 1984). The Rb-Sr age of FK-N was reported at 512 ± 30 Ma, with $^{87}Rb/^{87}Sr$ and $^{87}Sr/^{86}Sr$ ratios of 69.9 ± 4.1 and 1.2114 ± .0021, respectively (Jegal *et al.* 2022).

An alternative K-feldspar RM that could be used for *in situ* Rb-Sr dating via LA-ICP-MS/MS is NBS SRM 607. This

RM has been shown to have heterogenous $^{87}Rb/^{86}Sr$ and $^{87}Sr/^{86}Sr$ ratios that, however, seem to plot on the same isochron (see Nebel and Mezger (2006)). Note that NBS SRM 607 was not analysed in this study due to the lack of NP material from this RM, but further work on *in situ* Rb-Sr dating of SRM 607 as well as preparation of NP is underway and will be the focus of future work.

Methods

Sample preparation

The RMs GL-O, Mica-Mg, Mica-Fe and FK-N were prepared in this study as (i) pressed NP pellets and as (ii) flux-free glasses (postscript G1 or G2). The latter was prepared via fusion using a high-energy laser beam (see below). An additional sample of GL-O grains was also prepared as a polished-mount with glauconite grains embedded in epoxy resin. The Mica-Mg-NP and GL-O-NP were prepared at the Institute of Geosciences, Kiel University, Germany, whereas Mica-Fe-NP and FK-N-NP were supplied by J. Hogmalm and T. Zack (see Hogmalm *et al.* 2017). All NP pellets were manufactured following the method and protocols described by Garbe-Schönberg and Müller (2014).

The flux-free mineral glasses produced in this study were melted and fused by laser heating at the RSES Argon Facility in The Australian National University (ANU), using a Photon Machine 100 W Fusions 10.6 CO_2 laser system. Following the recent work of He *et al.* (2016), who aimed to produce flux-free glasses of silicate rocks in a furnace, this study tried to produce the glasses using an alternative and rather experimental laser-based approach for melting and fusion of silicates under ultra-high vacuum. In this study, two $\sim$ 10 mg portions of each material/mineral powder were loaded into miniature alumina crucibles, and then all crucibles were placed in the laser chamber under ultra-high vacuum. Mica-Mg, Mica-Fe and FK-N were loaded as powders whereas GL-O was loaded as mineral grains. Each portion was heated by moving the focussed laser beam over the surface of the samples located inside the crucible for 10–15 min. The actual temperature of the laser beam was unknown during the experiment, however, the melting of the samples was monitored by a camera installed inside the chamber. The laser energy was gradually increased until the targeted sample appeared to be molten. The laser beam was then turned-off to quench the melt and to produce a mineral glass. The maximum laser energy used for each sample is listed in Table 3.

Impact of laser-based melting/fusion on produced mineral glasses

The above RMs interacted differently with the laser beam during fusion due to their distinct physical properties and variable melting points. When the Mica-Mg and Mica-Fe powders were exposed to the laser beam, they produced melts with low viscosity that randomly spread at the bottom of the crucible (Figure 1). Portions of the melt migrated away from the area of the laser beam and incorporated un-melted powder, which translated to incomplete melting and inhomogeneities within the fused glasses. The produced glasses (Mica-Mg-G1 and G2, Mica-Fe-G1 and G2) were irregular in shape (Figure 1), with remnants of the mineral powders accumulated and preserved beneath the fused surface of the glasses. This is not surprising considering a relatively high melting point for micas that is typically in excess of 1100 °C (Gardien *et al.* 1995).

In contrast, the powdered sample of FK-N melted faster than Mica-Mg and Mica-Fe without any evidence of remnant mineral powder within the fused glass. FK-N powder produced a melt that accumulated at the bottom of the crucible. The FK-N produced glasses (FK-N-G1 and G2) were semi-spheroidal with a flat surface, and had a typical diameter of 1 mm (Figure 1).

GL-O glauconite grains required a slightly longer time (by about 2–3 min) to melt compared with other RMs presented as mineral powders. The GL-O melt accumulated at the centre of the crucible and then formed a semi-spheroidal glass with a flat surface and a typical diameter of about 1 mm (Figure 1). All produced mineral glasses contained random hollows and vesicles visible on the surface of fused glasses, which significantly limited the area that could be targeted for LA-ICP-MS/MS analysis. All fused mineral glasses were mounted in epoxy resin and polished before microscopic inspection and LA-ICP-MS/MS analysis (see below).

SEM/EDS Instrumentation

The fused mineral glasses were mapped for their major element compositions and homogeneity using a FEI Quanta 450 high-resolution field emission Scanning Electron Microscope (SEM), equipped with an energy dispersive X-ray spectrometer (EDS) detector at Adelaide Microscopy, University of Adelaide. In addition, higher-resolution imaging and mineral mapping was conducted on the GL-O grains at Macquarie University, using a FEI Teneo LoVac field emission SEM, equipped with EDS detectors (dual Bruker XFlash,

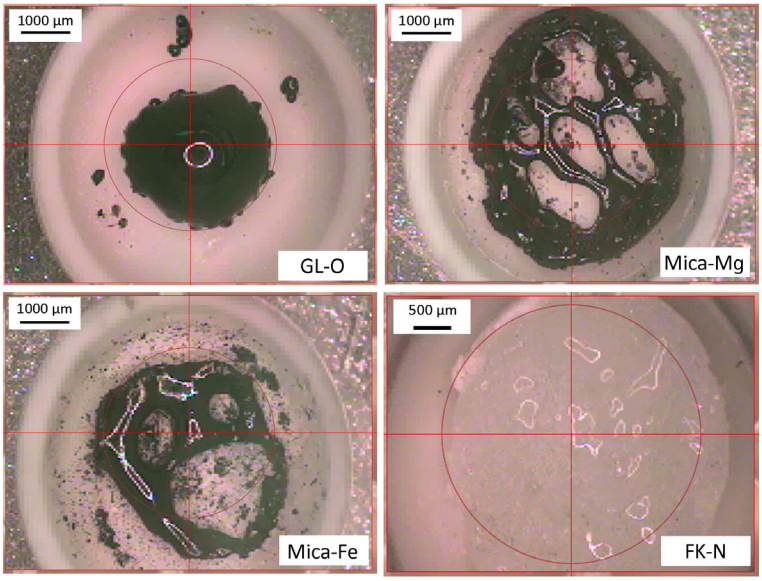

Figure 1. Images of fused glasses (top view) from GL-O, Mica-Mg, Mica-Fe (dark material) and FK-N (glassy material) contained in miniature alumina crucibles inside a laser chamber after experimental melting using a Photon Machine 100 W Fusion CO_2 laser system at the Ar-Ar laboratory in the Australian National University (ANU).

Series 6). The SEM/EDS setup at Macquarie University, coupled with Nanomin software for EDS spectra deconvolution and mineral identification (Rafiei *et al.* 2020), was used to investigate the micro-scale mineralogical heterogeneities and impurities within the GL-O grains.

LA-ICP-MS/MS Instrumentation

The mass fractions (µg g^{-1}) of Rb and Sr and some major elements (Si, K, Al, Fe and Mg) in the samples were measured simultaneously with $^{87}Rb/^{86}Sr$ and $^{87}Sr/^{86}Sr$ isotopic ratios using an Agilent 8900 ICP-MS/MS (with a collision/reaction cell) coupled with a RESOlution ArF excimer (193 nm) laser ablation system at Adelaide Microscopy, University of Adelaide. The first measurement session (Session 1) used a 74 µm laser spot and included Mica-Mg-NP, GL-O-NP, GL-O grains and MDC phlogopite. Measurement sessions 2 and 3 used a 67 µm laser spot and included the Mica-Mg-NP, GL-O-NP, Mica-Fe-NP, FK-N-NP as well as GL-O grains and MDC. Finally, GL-O-G1 and G2, Mica-Mg-G1, Mica-Fe-G1 and G2, and FK-N-G1 and G2 were analysed in Session 4, along with Mica-Mg-NP, Mica-Fe-NP and FK-N-NP, using a 74 µm laser spot. For each session, the LA-ICP-MS/MS was tuned using NIST SRM 612 glass, and the tuning parameters and instrument settings are listed in Table 2. All samples were ablated in a He atmosphere, mixed with Ar as the carrier gas, and an additional 3.5 ml min^{-1} of N_2 were added to enhance the signal sensitivity (Hu *et al.* 2008). N_2O gas was used as the reaction gas (0.35 ml min^{-1}) to resolve the isobaric interference between ^{87}Rb and ^{87}Sr using the collision/reaction cell. N_2O was used in preference to O_2 or SF_6 (Zack and Hogmalm 2016, Hogmalm *et al.* 2017) as Sr reacts with higher efficiency, resulting in higher signal intensities of measured SrO^x (Redaa *et al.* 2021). Mica-Mg-NP and NIST SRM 610 were used as primary RMs to normalise $^{87}Rb/^{86}Sr$ and $^{87}Sr/^{86}Sr$ ratios using a sample-calibrator-sample bracketing method (see Redaa *et al.* 2021). NIST SRM 610 was used to calibrate Rb and Sr mass fractions, with Al as the internal standard element. The $^{87}Rb/^{86}Sr$ and $^{87}Sr/^{86}Sr$ ratios were processed using the Iolite v4 software (Paton *et al.* 2011), coupled with a customised data reduction scheme for the Rb-Sr isotopic analysis available from https://forum.iolite.xyz/d/148-new-rb-sr-drs (Redaa *et al.* 2021). Rb-Sr data processing is described in detail in previous publications (Hogmalm *et al.* 2017, Laureijs *et al.* 2021, Redaa *et al.* 2021). Rb-Sr isochrons and ages were calculated using the IsoplotR software (Vermeesch 2018).

Rb-Sr isotope dilution by MC-ICP-MS

The Rb-Sr isotopic compositions for powders of phlogopite Mica-Mg and glauconite GL-O were determined by isotope dilution multi-collector inductively coupled plasma-mass spectrometry (MC-ICP-MS) at the University of Melbourne, using methods adapted from Maas *et al.* 2015 (see also Dalton

Table 2.
Laser ablation and ICP-MS/MS operating parameters

Laser parameters	Value
He carrier gas	380 ml min^{-1}
Ar carrier gas	880 ml min^{-1}
N_2 addition	3.5 ml min^{-1}
Spot size	74 or 67 μm
Repetition rate	5 Hz
Fluence	3.5 J cm^{-2}
Sample chamber	S155 large format
ICP-MS/MS	
Plasma parameters	
RF power	1350 W
Sample depth	5 mm
Lens parameters	
Extract 1	-2 V
Extract 2	-140 V
Omega bias	-80 V
Omega lens	7 V
Q1 entrance	1.5 V
Q1 exit	-2 V
Cell focus	-2 V
Cell entrance	-90 V
Cell exit	-120 V
Deflect	- 11 V
Plate bias	-80 V
Q1 parameters	
Q1 bias	-2 V
Q1 prefilter bias	-10 V
Q1 postfilter bias	-7 V
Cell parameters	
N_2O flow rate	0.35 ml min^{-1}
OctP bias	-23 V
Axial acceleration	2 V
OctP RF	180 V
Energy discrimination	-8 V
Q2 parameters	
Q2 bias	-31 V
Measured masses, mass shifts and dwell times (in brackets)	Mg24 - > 40 (2) amu (ms) Al27 - > 27 (2) amu (ms) Si29 - > 45 (2) amu (ms) K39 - > 39(2) amu (ms) Fe56 - > 72 (5) amu (ms) Rb85 - > 85 (5) amu (ms) Sr86 - > 102 (5) amu (ms) Sr87 - > 103 (5) amu (ms)

et al. 2020, Fiorentini *et al.* 2020). Aliquots (10–20 mg of Mica-MG, ~ 20 mg for GL-O) of the RMs were mixed with ^{85}Rb-^{84}Sr spike solution and digested at low pressure (3:1 HF: HNO_3, 100 °C, 48 h, pure HNO_3 and finally 6 mol l^{-1} HCl). Strontium and Rb were extracted and purified from the sample solutions using EICHROM™ Sr resin (0.15 ml bed 100–150 μm, two passes for Sr) and AG-W50-X8 (4 ml bed, 200–400 mesh), respectively. Procedural blanks (< 0.05 ng Rb, Sr) produced negligible blank corrections.

All analyses were carried out on a NU Plasma MC-ICP-MS. Strontium isotope data were acquired on total Sr signals of 8–10 V corrected for Sr memory and Kr-Rb isobaric interferences using a combination of a 30-s 'on-peak zero' baseline measurement before the sample was aspirated and within-run interference monitoring at masses 83 and 85; ^{87}Sr data acquired with > 0.3 mV of residual ^{85}Rb were corrected for ^{87}Rb interference using the measured $^{85}Rb/^{87}Rb$ (i.e., spiked). Sr mass bias was corrected by internal normalization to $^{88}Sr/^{86}Sr = 8.37521$ using the exponential law in an online iterative spike unmixing routine. Measurement repeatability precision (2SE) for means of thirty 10-s integrations was typically ±0.000020 (somewhat higher for radiogenic Sr such as Mica-Mg) and intermediate measurement precision ("external precision") was near ±0.000040 (2*s*). Data for $^{87}Sr/^{86}Sr$ are reported relative to a ratio of 0.71023 for NIST SRM 987; measured values for NIST SRM 987 were in the range 0.71018–0.71025, with smaller ranges in individual sessions. Rubidium isotope dilution analyses were done using Zr-doping (Waight *et al.* 2002); this produced corrected $^{85}Rb/^{87}Rb$ ratios for unspiked Rb in the range 2.590–2.593 and yielded $^{87}Rb/^{86}Sr$ with intermediate measurement precision of ±0.5% (2*s*).

Data quality for these isotope dilution results was examined using two reference materials, NIST SRM 607 K-feldspar and USGS basalt BCR-2. Two analyses of NIST SRM 607, with nominal $^{87}Rb/^{86}Sr$ = 24.26 and $^{87}Sr/^{86}Sr$ = 1.20048 (calculated from the certified Rb/Sr and $^{87}Sr/^{86}Sr$ after adjusting the certified to NIST SRM 987 = 0.71023), yield Rb-Sr model ages of 1442 and 1452 Ma, consistent with an age of 1447 ± 7 Ma obtained for the adjusted certified composition (initial $^{87}Sr/^{86}Sr$ = 0.705, Rb decay constant of Villa *et al.* 2015; see also Nebel and Mezger 2006). Rb-Sr data for six splits of two digestions of the BCR-2 basalt yield mean $^{87}Rb/^{86}Sr$ and $^{87}Sr/^{86}Sr$ of 0.3991 ± 0.0006 and 0.704986 ± 0.000019 (2*s*), respectively, consistent with reference data (e.g., http://georem.mpch-mainz.gwdg.de). Finally, Rb-Sr data for hornblende/augite and biotite from Mt Dromedary monzonite (NSW, SE Australia) yielded an isochron age of 99.27 ± 0.26 Ma (MSWD 1.3, $^{87}Sr/^{86}Sr_i$ 0.70450 ± 5, errors 95% CL). This age is consistent with CA-ID-TIMS zircon U-Pb age and $^{40}Ar/^{39}Ar$ biotite ages of *ca.* 99 Ma (see Phillips *et al.* 2017).

Results and discussion

Chemical and elemental homogeneity

The composition and spatial homogeneity of the fused glasses was firstly investigated using micro-scale elemental

maps generated by SEM/EDS. The elemental maps show the presence of K, Al, Si, Fe and Mg as major elements within the glasses as shown in online supporting information Figures S1–S5. In addition, GL-O glass contains traces of Ca and P (Figures S4–S5) that agrees with the presence of minor apatite phases/inclusions detected via Nanomin maps of the GL-O grains (see Figure S6). In addition, calcite and plagioclase have been identified in GL-O grains (Boulesteix *et al.* 2020).

The Rb and Sr mass fractions of the NP pellets and glasses were determined by LA-ICP-MS/MS, and the measurement results are listed in online supporting information Table S1, and summarised in Figures 2 and 3, and Table 3. The Rb mass fractions of all NP pellets agree with their published values within uncertainty. However, Sr in Mica-Mg, Mica-Fe and FK-N NPs is lower than the reference values (see Figure 3 and Table 3).

The glasses showed variation in their Rb and Sr mass fractions (μg g^{-1}) compared with the reported values for their equivalent powders. The measured Rb mass fractions for the glasses derived from powdered samples (Mica-Mg-G1, Mica-Fe-G1 and -G2, FK-N-G1 and -G2) are, on average, lower than the mass fractions measured in the corresponding NP pellets and have large uncertainties. The % RSD ranged between 3% and 28% (2*s*). The systematically lower Rb mass fractions in the glasses indicate that Rb was most likely lost during the melting process. Comparing the Rb mass fractions in Mica-Mg-G1 (product) and Mica-Mg-NP (source material) indicates a Rb loss of about 41%. The other glasses produced from Mica-Fe, GL-O and FK-N showed Rb loss between 1% and 15%. This variation in Rb losses between the glasses is probably due to the differences in the physical (i.e., grains *vs.* powder, melting point etc) and chemical properties (e.g., composition, amount of mineral water, etc) of the RMs, in addition

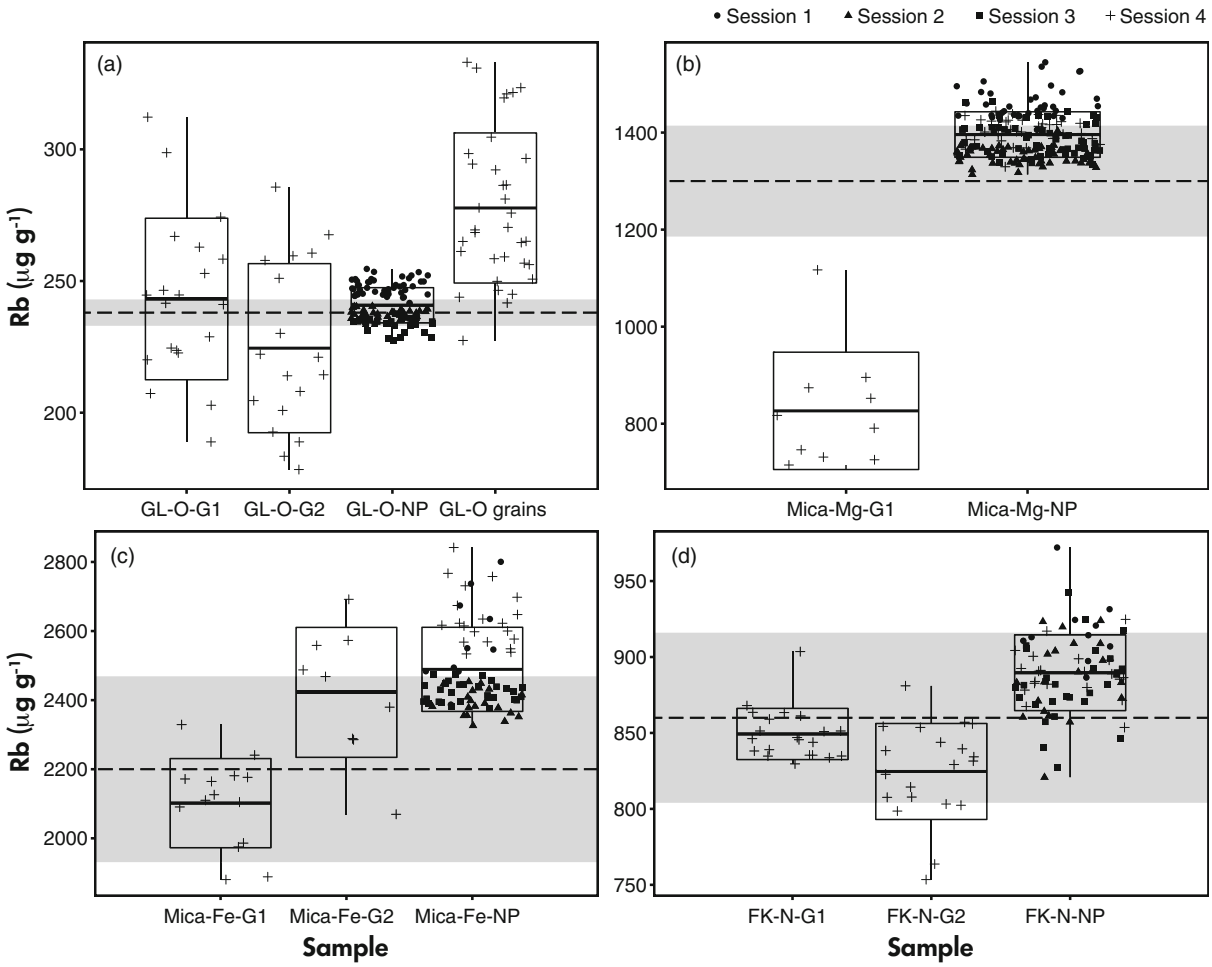

Figure 2. Boxplot diagrams showing measured Rb mass fractions in glasses and NPs from GL-O, Mica-Mg, Mica-Fe and FK-N RMs. The dashed line represents the Rb mass fraction (from published studies) with the shaded area illustrating the uncertainty (see data and references listed in Table 3).

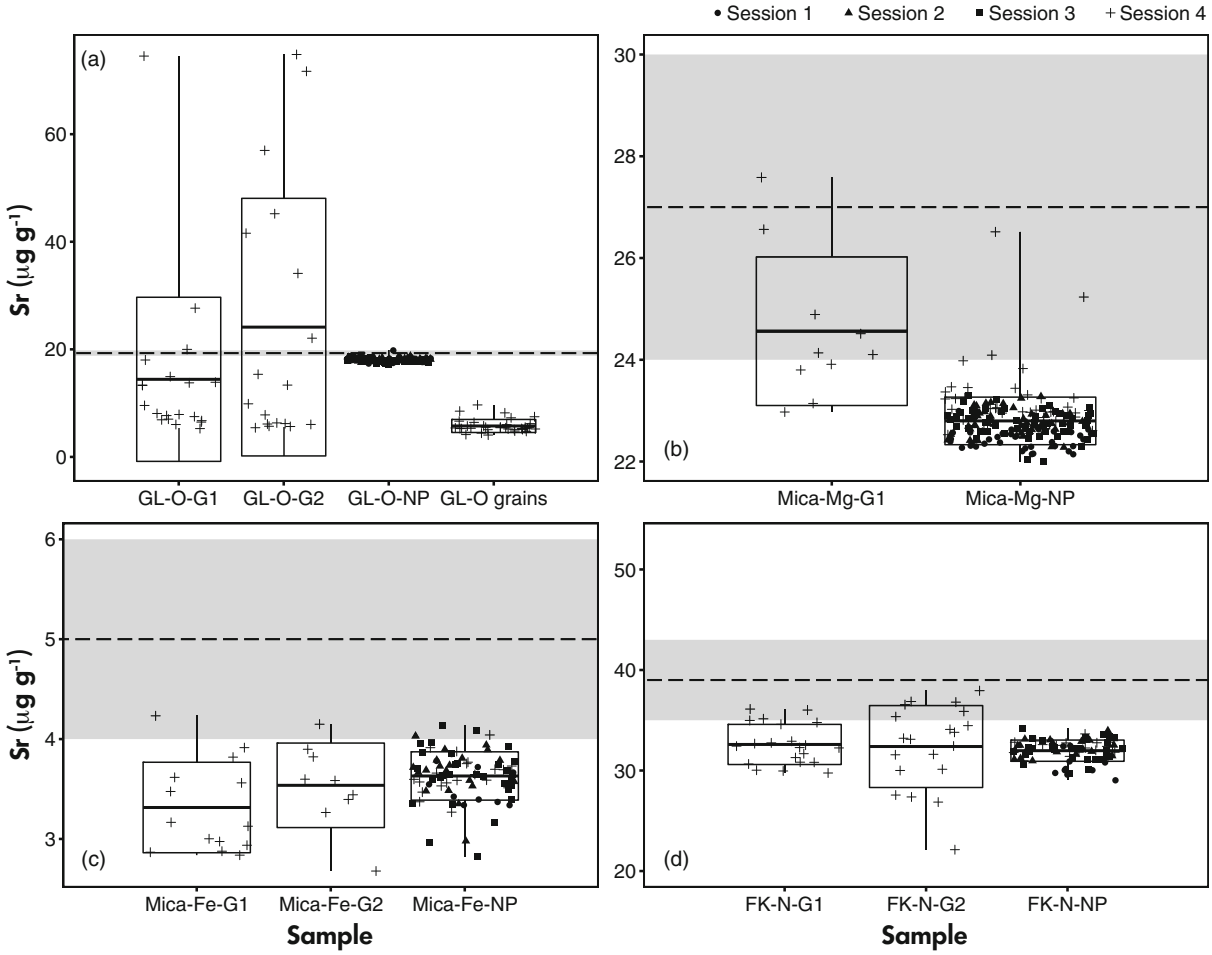

Figure 3. Boxplot diagrams with Sr mass fractions from GL-O, Mica-Mg, Mica-Fe and FK-N glasses and NPs. The dashed line represents the published Sr mass fraction with shaded area illustrating the uncertainty (see data and references listed in Table 3).

to the variation in the melting conditions related to the laser energy applied. For example, Rb loss is particularly obvious from Mica-Fe-G1 and FK-N-G2, which were melted at relatively higher laser outputs (3.1 W mm^{-2}) and, hence, temperatures. The temperature reached was not measured directly but it can be inferred that the melting points of the minerals tested were significantly higher than the boiling point of Rb (~ 688 °C), but lower than the boiling point of more refractory Sr (1382 °C, Gray 2009).

The Sr mass fractions in Mica-Mg-G1, Mica-Fe-G1 and -G2, and FK-N-G1 and -G2 agree within uncertainty of the published mass fractions for these minerals (see Figure 3). This general agreement indicates that Sr did not volatilise significantly during the melting process, which suggests that the fusion temperature did not exceed the boiling point of Sr. However, the mineral glasses were more heterogeneous for Sr compared with the NP pellets, which could be due to incomplete mixing of mineral heterogeneities during fusion. This can be also explained by the additional homogenisation of the NP during milling prior to pressing into pellets, compared with the source mineral powders, which were used to produce the glasses.

The mean Rb mass fraction of the GL-O grains was higher than in GL-O-NP by about 15–25% (see Figure 2). In contrast, Sr mass fractions were lower in the GL-O grains compared with the NP by 60–77% (see Figure 3). We speculate that this marked difference in Sr mass fractions is due to the presence of mineral inclusions (particularly apatite and calcite), which were avoided during LA-ICP-MS/MS analysis. Here, analysis primarily targeted centres of the grains, while avoiding mineral inclusions which are more abundant in rims or outer areas of glauconite grains. A corresponding difference was also observed for Ca mass fractions between GL-O grains and GL-O-NP, with Ca being 60% lower in the grains, which supports the incorporation of

Table 3.
Rubidium and Sr mass fractions of glasses and NPs analysed by LA-ICP-MS/MS. The second column shows the maximum laser output used to melt the glasses

Sample	Maximum laser Energy ($W\ mm^{-2}$)	Session	Rb ($\mu g\ g^{-1}$)	2*s*	% RSD	Expected Rb	Sr ($\mu g\ g^{-1}$)	2*s*	% RSD	Expected Sr	*n*
FK-N-NP		Session 1	917.75	45.19	4.92	860 ± 50*	30.52	2.25	7.37	39 ± 4*	10
FK-N-NP		Session 2	886.38	51.32	5.79		32.34	1.59	4.9		20
FK-N-NP		Session 3	882.7	48.02	5.44		32.06	2.03	6.34		29
FK-N-NP		Session 4	888.96	30.94	3.48		32.2	1.28	3.98		21
		mean	889.64	48.87	5.49		31.97	2.07	6.47		80
FK-N-G1	1.85	Session 4	849.32	33.01	3.89		32.59	3.91	12		21
FK-N-G2	3.1	Session 4	824.63	61.94	7.51		32.39	7.99	24.66		20
GL-O-NP		Session 1	247.83	5.86	2.36	238 ± 5#	18.13	0.72	4	19.3 ± 0.5#	46
GL-O-NP		Session 2	237.71	2.85	1.2		18.1	0.53	2.94		34
GL-O-NP		Session 3	233.51	5.11	2.19		17.92	0.82	4.55		30
		mean	240.8	13.09	5.44		18.07	0.71	3.95		110
GL-O		MC-ICP-MS	237.11	16.50**	6.96**		18.84	1.31**	6.96**		16
GL-O grains		Session 1	305.04	83.08	27.24		4.86	1.71	35.11		
GL-O grains		Session 2	288.29	41.47	14.39		5.25	2.3	43.85		
GL-O grains		Session 3	296.48	73.89	24.92		4.37	1.64	37.56		
GL-O grains		Session 4	277.74	55.86	20.11		5.75	2.38	41.33		
GL-O-G1	2.5	Session 4	243.18	60.11	24.72		14.43	29.9	207.27		20
GL-O-G2	4.3	Session 4	224.5	62.92	28.03		24.13	46.93	194.5		18
Mica-Fe-NP		Session 1	2579.1	253.42	9.83	2200 ± 80&	3.54	0.38	10.86	5 ± 1&	10
Mica-Fe-NP		Session 2	2393.39	76.08	3.18		3.67	0.46	12.53		20
Mica-Fe-NP		Session 3	2423.57	54.69	2.26		3.63	0.58	15.87		30
Mica-Fe-NP		Session 4	2638.09	163.87	6.21		3.64	0.35	9.73		20
		mean	2489.1	238.67	9.59		3.63	0.47	13.06		80
Mica-Fe-G1	3.1	Session 4	2101.86	252.88	12.03		3.31	0.89	26.78		14
Mica-Fe-G2	2.5	Session 4	2422.47	368.67	15.22		3.54	0.83	23.44		9
Mica-Mg-NP		Session 1	1461.59	65.43	4.48	1300 ± 40&	22.46	0.42	1.85	27 ± 3&	37
Mica-Mg-NP		Session 2	1351.53	33.24	2.46		22.77	0.46	2.03		51
Mica-Mg-NP		Session 3	1387.11	63.7	4.59		22.76	0.5	2.19		57
Mica-Mg-NP		Session 4	1404.56	46.79	3.33		23.23	1.44	6.19		39
		mean	1395.92	91.94	6.59		22.8	0.92	4.02		184
Mica-Mg		MC-ICP-MS	1222	5	0.41		25.93	0.03	0.12		4
Mica-Mg-G1	3.1	Session 4	826.46	237	28.68		24.56	2.86	11.65		10

* Govindaraju and Roelandts (1988).
& Govindaraju (1995).
# Govindaraju (1995), Odin (1976).
** This relatively high uncertainty indicates natural heterogeneity between the aliquots, compared with the analytical uncertainty of 0.5%.

Sr-rich, Ca-bearing inclusions such as calcite or apatite (see data in Table S1).

The observed spread in Rb mass fractions in GL-O grains likely represents natural variation between individual glauconite grains (see also data in Odin *et al.* 1982), coupled with the effects of mixing (i) Rb-rich 'pure' glauconite zones with (ii) Rb-poor impurities (calcite, apatite). The complex mineralogy of single GL-O grains highlights the advantage and importance of the *in situ* Rb-Sr dating approach via LA-ICP-MS/MS as this technique can avoid possible contamination of younger diagenetic mineral phases or older detrital phases and micro-inclusions (Scheiblhofer *et al.* 2022).

The mean Sr mass fractions of the GL-O-G1 and -G2 glasses are within uncertainty of the bulk powdered GL-O reference values but they are also heterogeneous (> 24% RSD and ~ 200% RSD for Rb and Sr, respectively, 2*s*, see Table 3 and Figure 3). As mentioned above, the heterogeneity of the GL-O glasses are also probably due to the presence of minor apatite and calcite impurities, which have been homogenised in the GL-O powder compared with the fused glass produced from heterogeneous mineral grains.

The elemental homogeneity of the glasses and NPs was assessed at the micro-scale for major elements as well as Sr and Rb, using LA-ICP MS/MS and following the approach described in Gilbert *et al.* (2013). This approach compares

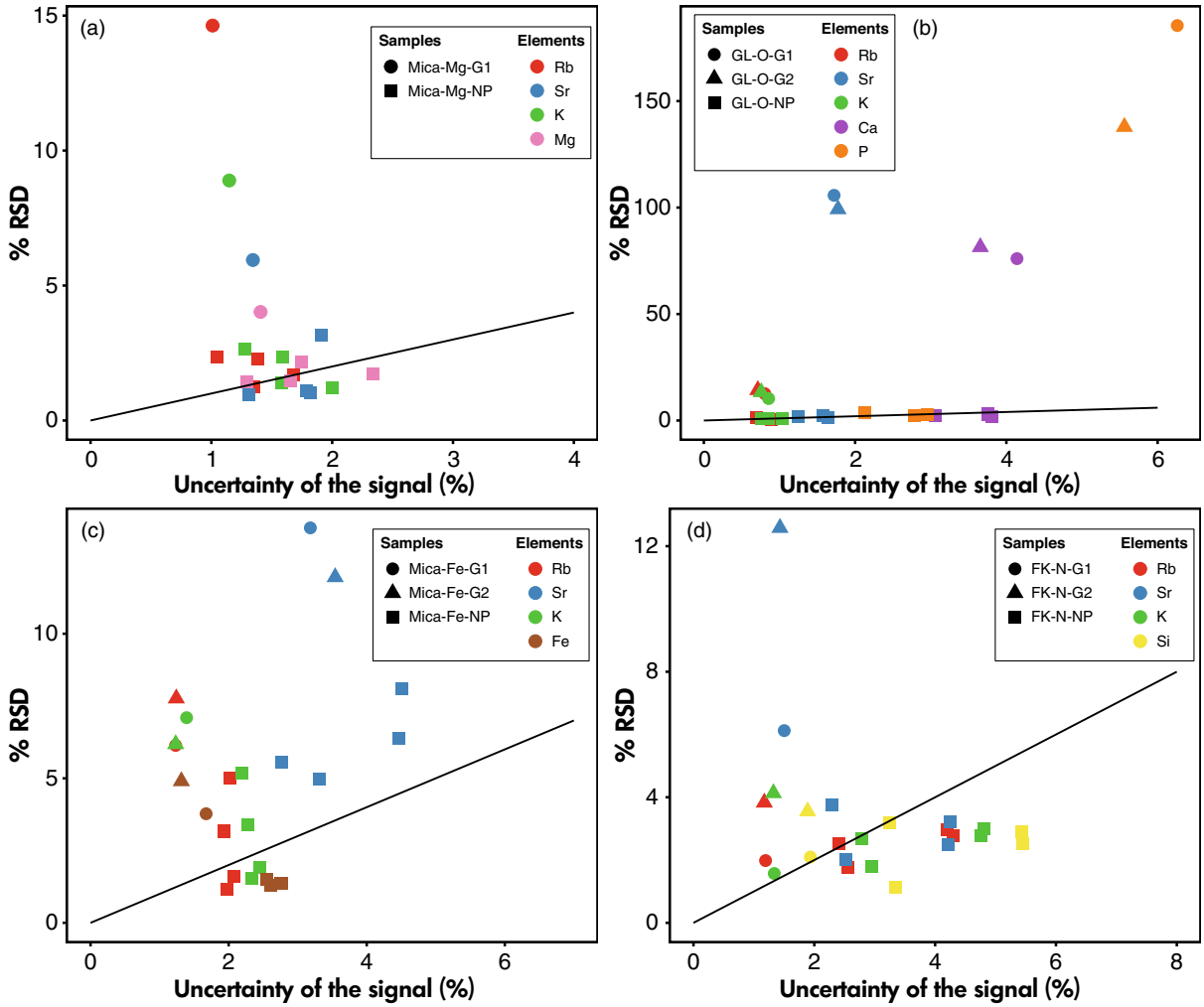

Figure 4. Cross-plots of relative standard deviation (% RSD) of multiple analyses (LA-ICP-MS/MS) versus the uncertainty of the signal u(S), which can be used to assess the homogeneity of RMs at the micro-scale (following the approach of Gilbert *et al.* 2013). The black line shows 1:1 trend between these two variables (% RSD and u(S)); if a studied material was completely homogeneous then all data would plot ideally along this line.

the uncertainty of the element signal u(S) with the uncertainty of measurement repeatability (% RSD) within a measurement session (Figure 4). These uncertainties are theoretically equal if the investigated sample is homogeneous, but when the % RSD is significantly greater than u(S) then the element distribution is considered heterogeneous (Gilbert *et al.* 2013). The LA-ICP-MS/MS data show that the glasses are heterogeneous for most major elements, Rb and Sr, and especially Ca, P and Sr in GL-O glasses (Figure 4). On the other hand, Mica-Mg-NP, GL-O-NP and FK-N-NP were more homogeneous with % RSD of 4% or less (Figure 4). Conversely, Mica-Fe-NP is the least homogeneous of the NP materials with high internal variations for Sr (5–8% RSD), and Rb and K in some sessions. Finally, FK-N-NP tended to produce the noisiest signals with high u(S) in some sessions. Calcium and P have higher u(S) than other elements in GL-O-NP but were homogeneously distributed in this NP (on the 1:1 line, Figure 4b). Although Ca and P are primarily hosted in the minor apatite and calcite phases in the sample, they are distributed evenly within the GL-O-NP.

Assessment of $^{87}Rb/^{86}Sr$ and $^{87}Sr/^{86}Sr$ isotope homogeneity via LA-ICP MS/MS

To investigate the homogeneity of $^{87}Rb/^{86}Sr$ and $^{87}Sr/^{86}Sr$ ratios and to assess the potential of each material to be used as RMs, the ratios were normalised to NIST SRM 610 (see Redaa *et al.* 2021). Although the $^{87}Rb/^{86}Sr$ ratios are not corrected for matrix effects, and the absolute ratios are biased, this approach allows for an assessment of homogeneity for all materials including Mica-Mg-NP. The

Table 4.
Mean $^{87}Rb/^{86}Sr$ and $^{87}Sr/^{86}Sr$ ratios analysed by LA-ICP-MS/MS and normalised to NIST SRM 610, and solution MC-ICP-MS

Sample	Session	$^{87}Rb/^{86}Sr$	2*s*	% RSD	$^{87}Sr/^{86}Sr$	2*s*	% RSD	*n*
FK-N-NP	Session 1	84.9	4.75	5.6	1.213	0.014	1.12	10
FK-N-NP	Session 2	77.57	4.3	5.54	1.216	0.023	1.9	20
FK-N-NP	Session 3	78.27	4.87	6.22	1.217	0.024	1.98	29
FK-N-NP	Session 4	77.97	2.87	3.68	1.212	0.017	1.4	21
	mean	79.68	6.85	8.59	1.215	0.005	0.38	4
FK-N-G1	Session 4	73.8	9.82	13.31	1.22	0.05	4	21
FK-N-G2	Session 4	73.08	17.14	23.46	1.23	0.07	5	20
GL-O-NP	Session 1	38.69	1.78	4.6	0.755	0.0141	1.86	46
GL-O-NP	Session 2	37.21	1.28	3.4	0.7561	0.0153	2.03	34
GL-O-NP	Session 3	36.25	1.69	4.7	0.753	0.0172	2.29	30
	mean	37.4	2.41	6.44	0.7547	0.0031	0.4	3
GL-O	MC-ICP-MS	36.57	0.26	0.71	0.753561	0.00032	0.04	16
GL-O grains	Session 1	183.9	73	39.7	0.933	0.088	9.4	18
GL-O grains	Session 2	162	52.1	32.2	0.919	0.082	8.9	14
GL-O grains	Session 3	200	54.4	27.2	0.97	0.082	8.5	18
GL-O grains	Session 4	140.4	40.2	28.7	0.884	0.055	6.2	68
GL-O-G1	Session 4	74.27	76.53	103	0.805	0.103	12.79	20
GL-O-G2	Session 4	65.25	98.98	152	0.792	0.128	16.19	18
Mica-Fe-NP	Session 1	2067	148	7.17	7.8	0.64	8.22	10
Mica-Fe-NP	Session 2	1906	264	13.85	8.07	0.99	12.24	20
Mica-Fe-NP	Session 3	1956	342	17.47	8.14	1.22	15.05	30
Mica-Fe-NP	Session 4	2072	196	9.46	7.97	0.7	8.8	20
	mean	2000.2	161.8	8.1	8	0.29	3.62	4
Mica-Fe-G1	Session 4	1837	354	19.28	8.57	0.88	10.24	14
Mica-Fe-G2	Session 4	2001	691	34.56	8.49	0.64	7.6	9
Mica-Mg-NP	Session 1	183.8	7.9	4.3	1.8509	0.0173	0.93	37
Mica-Mg-NP	Session 2	168.1	4.1	2.42	1.8608	0.0339	1.82	51
Mica-Mg-NP	Session 3	172.7	7.7	4.49	1.8647	0.0365	1.96	60
Mica-Mg-NP	Session 4	171.2	12.5	7.29	1.8522	0.0258	1.39	39
	mean	173.9	13.5	7.71	1.857	0.013	0.7	4
Mica-Mg	MC-ICP/MS	151.4	0.54	0.36	1.8406	0.0002	0.01	4
Mica-Mg-G1	Session 4	96	33	34.49	1.84	0.11	5.7	10
BCR-2G	Session 1	0.445	0.021	4.8	0.7048	0.0024	0.34	26
	Session 2	0.421	0.013	3.1	0.7055	0.004	0.57	26
	Session 3	0.407	0.008	2.1	0.7048	0.0053	0.75	34
	Session 4	0.419	0.15	3.6	0.70508	0.0048	0.69	26
	Mean	0.4227	0.031	7.28	0.70505	0.00065	0.09	4

Note that $^{87}Rb/^{86}Sr$ ratios acquired by LA-ICP-MS/MS are biased and not comparable due to the matrix effect, but were listed here to illustrate their variations between and within sessions.

measurement results are listed in Table S2, summarised in Table 4 and plotted on 'Nicolaysen diagrams' (Figure 5).

GL-O glauconite: The normalised $^{87}Rb/^{86}Sr$ and $^{87}Sr/^{86}Sr$ ratios for GL-O are plotted with an initial Sr isotope ratio ($^{87}Sr/^{86}Sr_i$) of 0.70740 (Figure 5a). The latter represents the expected Sr isotope composition of seawater at 95–100 Ma (Veizer *et al.* 1999 and references therein, McArthur *et al.* 2012) when the glauconite is expected to have formed in marine settings from palaeo-seawater or coeval seawater-derived fluids.

The GL-O-NP is more homogeneous than Mica-Fe-NP, Mica-Mg-NP or FK-N-NP, with a mean $^{87}Rb/^{86}Sr$ of 37.4 ± 0.26 (2*s*) and $^{87}Sr/^{86}Sr$ of 0.7547 ± 0.0031 (2*s*); and reproducibility between the three sessions of 6.4% and 0.40% (% RSD, 2*s*), respectively. The measured $^{87}Sr/^{86}Sr$ of GL-O-NP (0.7547 ± 0.0031) is within uncertainty of the reported ratio of 0.7535 ± 0.001 (Govindaraju 1995, Odin 1976).

In comparison, both the fused glasses and the natural GL-O grains were highly variable with respect to their $^{87}Rb/^{86}Sr$ and $^{87}Sr/^{86}Sr$ ratios (Figure 5a), with the majority of GL-O data (from NP, glasses and grains) plotting along a single isochron (Figure 5a). As discussed above the GL-O grains are complex and composed of glauconite and other minor, Rb-poor and Sr-rich mineral phases (i.e., apatite, calcite and plagioclase). Therefore, the isochron for the GL-O materials in part reflects (i) natural Rb variation between

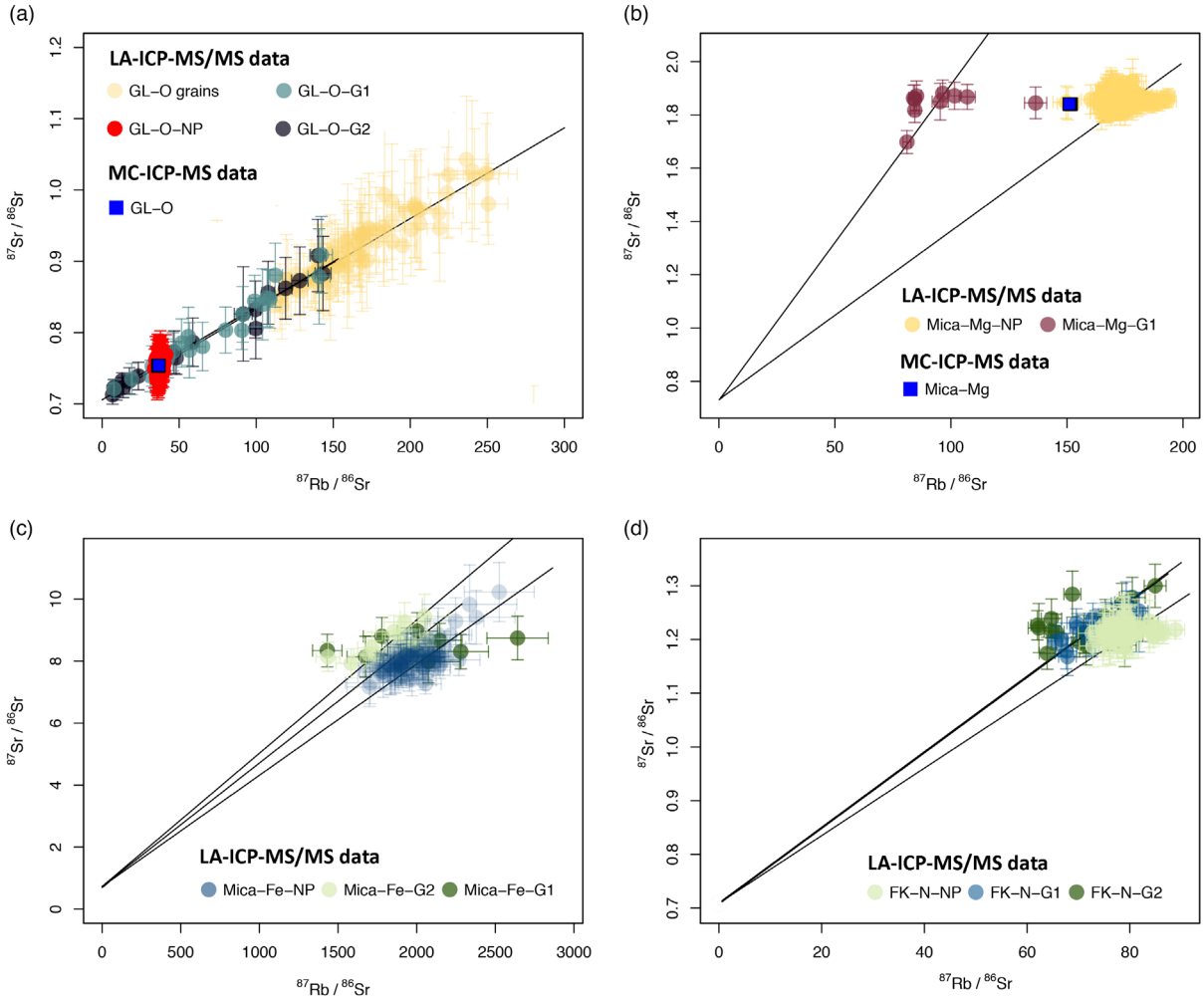

Figure 5. Rb-Sr isochron plots (Nicolaysen diagrams), constructed using IsoplotR (Vermeesch 2018), showing measured variations in $^{87}Rb/^{86}Sr$ and $^{87}Sr/^{86}Sr$ ratios in the fused mineral glasses (G1, G2 data) and nano-powder pelles (NP). Data were acquired via LA-ICP-MS/MS and normalised to NIST SRM 610 for the following minerals: (a) GL-O (Glauconite), (b) Mica-Mg (Phlogopite), (c) Mica-Fe (Biotite) and (d) FK-N (Potash Feldspar). These results are complemented by a high-precision isotope dilution (ID) Rb-Sr data from Mica-Mg and GL-O mineral powders (see blue squares) acquired by a solution-based MC-ICP-MS approach. However, $^{87}Rb/^{86}Sr$ data of the NPs is biased due to the matrix effect and not directly comparable.

grains (Nebel and Mezger 2006, Odin *et al.* 1982) and also (ii) a 'mixing line' between the glauconite and other Sr-rich phases. The Sr mass fractions and $^{87}Sr/^{86}Sr$ ratios of GL-O materials were plotted on a cross-plot (Figure 6; Langmuir *et al.* 1978) to investigate possible mixing phenomena between glauconite and other phases. The GL-O glasses (GL-O-G1 and G2) plot along a two-component mixing curve (Figure 6), with a systematic decrease in $^{87}Sr/^{86}Sr$ ratios with increasing Sr mass fractions ($\mu g\ g^{-1}$). In contrast, GL-O-NP did not show obvious variability, which is not surprising considering the higher homogeneity of the NP material compared with the glasses (see previous section).

In Figure 6b, the $^{87}Sr/^{86}Sr$ ratios were plotted against 1/Sr mass fraction for GL-O fused glasses with a linear trend fitted by IsoplotR (Vermeesch 2018) and using the least-squares algorithm of York *et al.* (2004). The projected $^{87}Sr/^{86}Sr$ *y*-intercepts of the regression lines are 0.70478 ± 0.011 (2SE) for GL-O G1 glass, and 0.70613 ± 0.0063 (2SE) for GL-O G2 (Figure 6b), which are within uncertainty the expected $^{87}Sr/^{86}Sr_i$ of 0.70740 (McArthur *et al.* 2012). The fact that all data from GL-O-G1 and G2 glasses, GL-O grains and GL-O-NP plot together along a common isochron (Figure 5a) suggest that all phases are coeval and formed via common early diagenetic

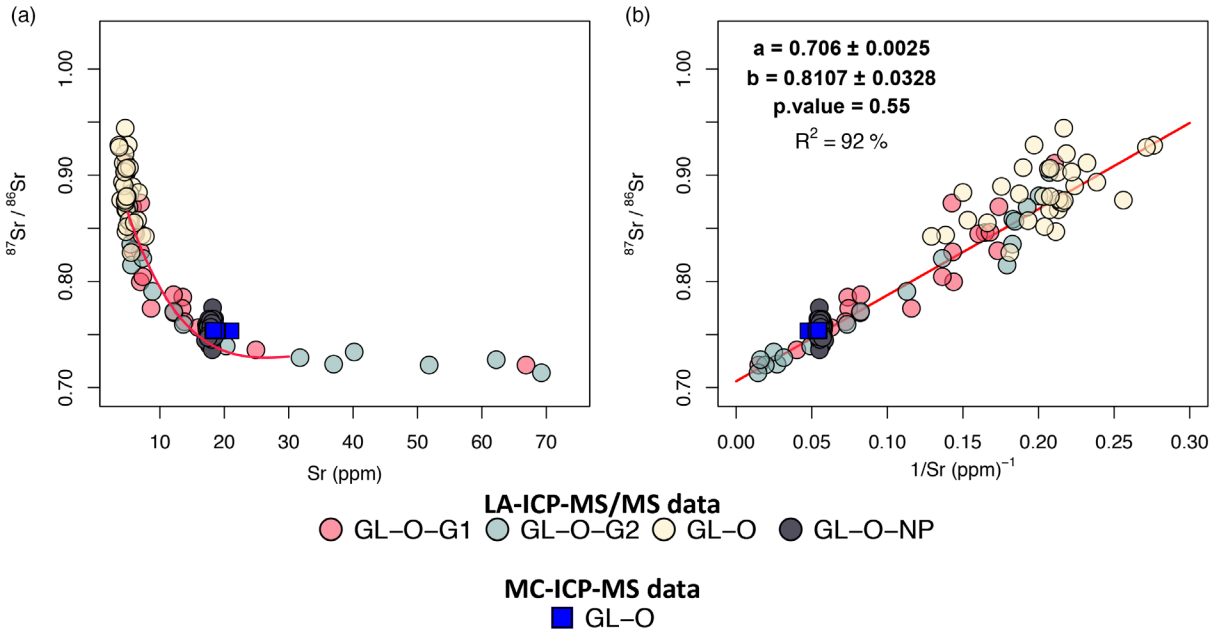

Figure 6. (a) Cross-plot of $^{87}Sr/^{86}Sr$ ratios vs. Sr mass fractions from GL-O glasses, GL-O grains and GL-O-NP nano-powder acquired via LA-ICP-MS/MS (circles), plotted along with a two-component theoretical mixing line (red curve). (b) Cross plot of $^{87}Sr/^{86}Sr$ vs. 1/Sr data showing statistically significant linear correlation. The LA-ICP-MS/MS data are complemented by a high-precision isotope dilution (ID) Rb-Sr data from GL-O mineral powders (see blue square) acquired by solution-based MC-ICP-MS.

process(es) in a marine setting. Hence, we argue that the Rb-Sr isotope system of GL-O glauconite grains, including minor apatite and calcite inclusions, has not been reset since the early diagenetic (authigenic) formation of the glauconite-apatite mineral assemblages. Considering its homogeneity, we propose that the produced GL-O-NP is a suitable RM for *in situ* Rb-Sr dating of glauconite, illite and/or micas. Further improvements could be made to produce an even more 'pure' and homogeneous glauconite NP by treating the source GL-O powder with weak acid that can dissolve the minor calcite and apatite impurities, prior to milling (Smalley *et al.* 1989).

Mica-Mg phlogopite: The mean $^{87}Rb/^{86}Sr$ ratios normalised to NIST SRM 610 are variable between sessions (ranging from 168 to 184, see Table 4 and Figure 7) with Session 4 being the most variable (7% RSD), and the other sessions being more homogeneous and comparable to GL-O-NP (2.4–4.5% RSD, 2*s*) (see Table 4 and Figure 7). The $^{87}Sr/^{86}Sr$ ratios of Mica-Mg-NP were more consistent between the sessions (% RSD = 0.7, 2*s*, *n* = 4), but the mean of 1.857 ± 0.013 (2*s*, *n* = 4) is lower than the $^{87}Sr/^{86}Sr$ reported in Olierook *et al.* (2020) by 0.65%, and higher than the value reported in Hogmalm *et al.* (2017) by 0.24% (see Table 1). This variation either reflects isotopic differences between batches of Mica-Mg, or inter-laboratory variability. Mica-Mg-G1 is highly variable and has systematically lower $^{87}Rb/^{86}Sr$ ratios by up to 40% compared with Mica-Mg-NP (Figure 5a), which most likely reflects a progressive loss of Rb during the formation of the fused mineral glass. Although the mean $^{87}Sr/^{86}Sr$ value of Mica-Mg-G1 (1.842 ± 0.11, 2*s*, *n* = 10) overlapped the expected ratios of Mica-Mg-NP (1.84 and 1.87, see Table 1), it is associated with a relatively high uncertainty (5% RSD, 2*s*), which is due to the heterogeneity of Mica-Mg-G1 in regards to $^{87}Sr/^{86}Sr$. Therefore, the Mica-Mg-G1 glass is unsuitable as a RM for *in situ* Rb-Sr dating. However, Mica-Mg-NP is a suitably homogeneous RM for *in situ* Rb-Sr dating of phlogopite and related mica group minerals (Hogmalm *et al.* 2017, Olierook *et al.* 2020, Redaa *et al.* 2021).

Mica-Fe biotite: The $^{87}Rb/^{86}Sr$ ratios of Mica-Fe-G1 and G2 are generally lower than of Mica-Fe-NP (Figure 5b) and have larger uncertainties of 19% RSD and 35% RSD (2*s*) for G1 and G2 glasses, respectively (Table 4). The decrease in $^{87}Rb/^{86}Sr$ ratios in the glasses, compared with Mica-Fe-NP (Figure 5c), confirms the loss of Rb from volatilisation during the melting process. The mean $^{87}Sr/^{86}Sr$ ratios of Mica-Fe-G1 and G2 are the same within

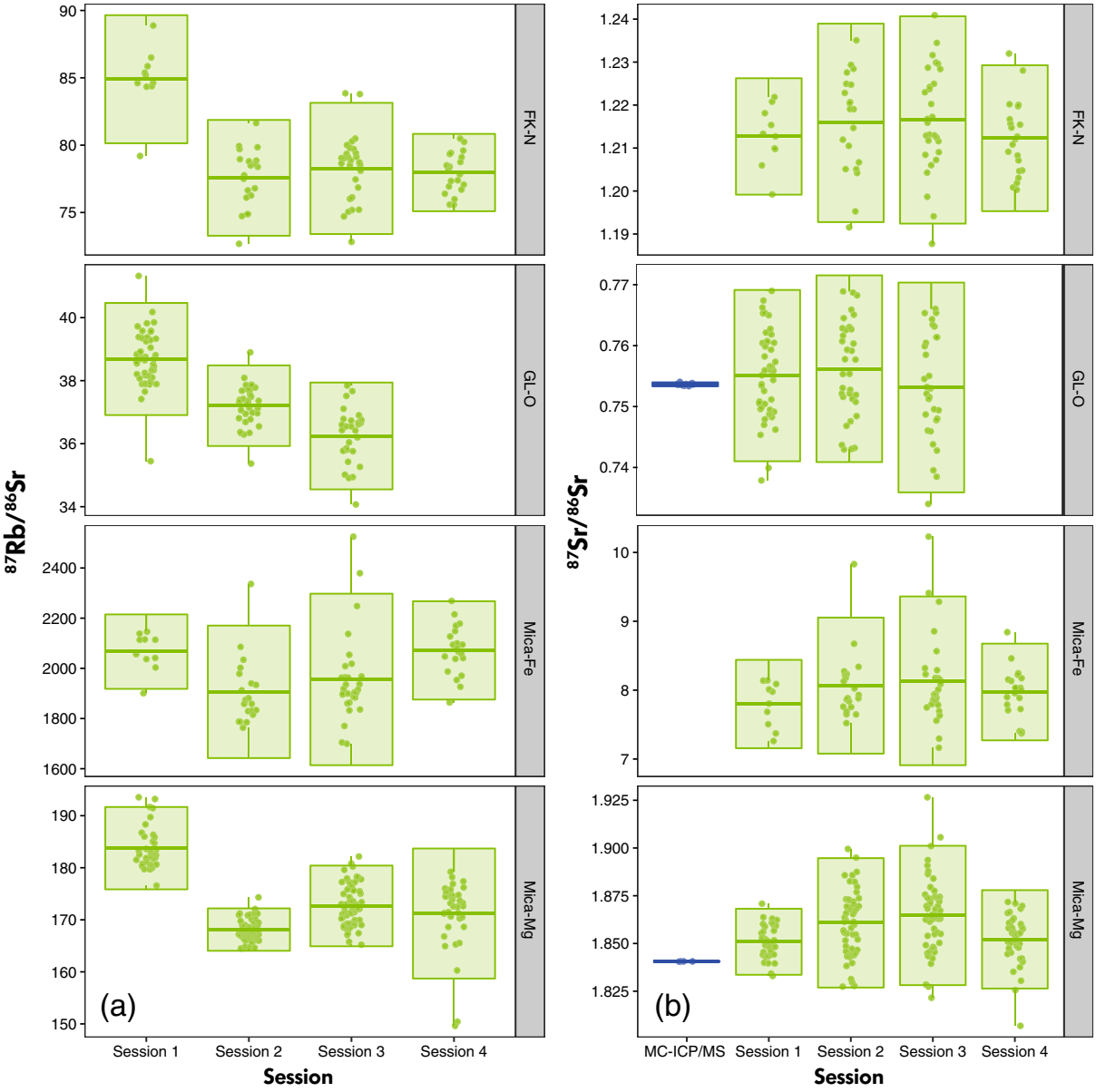

Figure 7. Variability in measured $^{87}Rb/^{86}Sr$ and $^{87}Sr/^{86}Sr$ ratios (left (a) vs. right (b) columns, respectively) analysed by LA-ICP-MS/MS (for different sessions: 1 to 4; see green data), and also via ID solution MC-ICP-MS (for GL-O and Mica-Mg and $^{87}Sr/^{86}Sr$ only, see blue data in (b) (right)). All *in situ* Rb-Sr isotopic ratios measured in the nano-powder pellets (FK-N-NP, GL-O-NP, Mica-Fe-NP, Mica-Mg-NP) were normalised to NIST SRM 610; thus, $^{87}Rb/^{86}Sr$ values presented in green in (a) are biased due to the matrix effect but presented here to compare variability between and within LA-ICP-MS/MS sessions. The boxes illustrate the mean and the standard deviation (95% confidence interval) of $^{87}Rb/^{86}Sr$ and $^{87}Sr/^{86}Sr$ ratios. Note that for LA-ICP MS/MS data from Sessions 1 and 4 were analysed with a 74 μm laser spot size, whereas the spot size of 67 μm was used for Sessions 2 and 3.

uncertainty (4% RSD, 2*s*), and are also in good agreement with the mean $^{87}Sr/^{86}Sr$ of Mica-Fe-NP analysed in the same session (Session 4) (see Figure 5c). The heterogeneous nature of the Mica-Fe glasses means they are not suitable as RMs for LA-ICP-MS/MS analysis. Mica-Fe-NP is also heterogeneous for both $^{87}Rb/^{86}Sr$ and $^{87}Sr/^{86}Sr$ ratios with reproducibility between the sessions estimated at 8% RSD and 3.6% RSD (2*s*, n = 4), respectively (see Table 4, and Figures 5 and 7). Due to this heterogeneity, Mica-Fe-NP is unsuitable as a primary RM for *in situ* Rb-Sr dating. However, all data plot along an isochron, so that Mica-Fe-NP could be used as a secondary RM (assuming its age is 287 ± 55

Ma (Jegal *et al.* 2022)) to monitor overall data quality and possible matrix effects, especially for biotite samples. Due to the large uncertainty associated with the reported age for Mica-Fe in Jegal *et al.* (2022), further characterisation for this sample is required to improve the uncertainty.

FK-N K-feldspar: Measured $^{87}Rb/^{86}Sr$ and $^{87}Sr/^{86}Sr$ ratios of FK-N (K-feldspar; FK-N-G1 and G2 glasses and NP) were normalised to NIST SRM 610, and the results are reported in Table S2 and summarised in Table 4. The $^{87}Rb/^{86}Sr$ ratios in the FK-N-G1 and G2 fused glasses broadly overlap but are lower on average than the ratios in the FK-N-NP (Figure 5d). Again, this indicates volatilisation and loss of Rb from the feldspar during melting. Conversely, $^{87}Sr/^{86}Sr$ ratios in the FK-N-G1 and -G2 are within uncertainty of FK-N-NP (Figure 5c). FK-N-NP is also heterogeneous for $^{87}Rb/^{86}Sr$ at micro-scale level with variation between sessions constrained at 8.59% (2*s*), but this variation is much smaller for $^{87}Sr/^{86}Sr$ (0.4%, 2*s*), see Table 4 and Figure 7). Based on these results, the FK-N RM is currently not suitable for the *in situ* Rb/Sr dating due to $^{87}Rb/^{86}Sr$ heterogeneity and the poorly constrained age and geological context.

Suitability of nano-powders (NP) for *in situ* Rb-Sr dating: Overall, our results show the Mica-Mg-NP and GL-O-NP to be homogeneous with respect to $^{87}Rb/^{86}Sr$ and $^{87}Sr/^{86}Sr$, indicating they could be suitable RMs for *in situ* Rb-Sr dating. However, the recommended $^{87}Rb/^{87}Sr$ and $^{87}Sr/^{86}Sr$ ratios of Mica-Mg reported in the literature are variable (see below, and data in Table 1). The recommended $^{87}Rb/^{86}Sr$ ratio for GL-O-NP has not been previously reported, and the published data (ID-TIMS) from GL-O powders and grains are also variable (see Odin *et al.* 1982, Jegal *et al.* 2022). Recent studies (e.g., Hogmalm *et al.* 2017) calculated the expected $^{87}Rb/^{86}Sr$ ratios of a given RM using (i) measured $^{87}Sr/^{86}Sr$ ratios normalised to NIST SRM 610, (ii) the expected age of the RM and (iii) its assumed initial $^{87}Sr/^{86}Sr$ ratio based on a cogenetic low Rb/Sr mineral, using the ^{87}Rb decay constant of $1.3972 \pm 0.0045 \times 10^{-11}$ (Villa *et al.* 2015). In this work, the $^{87}Rb/^{86}Sr$ ratios of Mica-Mg-NP and GL-O-NP were calculated using the above approach, and the mean $^{87}Sr/^{86}Sr$ ratios determined in multiple measurement sessions (listed in Table 4). BCR-2G glass was analysed as a secondary RM for $^{87}Sr/^{86}Sr$. The mean $^{87}Sr/^{86}Sr$ ratio for BCR-2G, determined over four measurement sessions, is 0.70505 ± 0.00065 (2*s*, $n = 4$), which agrees within uncertainty with the published $^{87}Sr/^{86}Sr$ reference value of 0.705003 ± 0.000008 (Elburg *et al.* 2005). Following the above approach, the $^{87}Rb/^{86}Sr$ of Mica-Mg-NP was calculated at 155.27 ± 2.0 (2*s*, propagated as described in Redaa *et al.* (2021)), based on the mean $^{87}Sr/^{86}Sr$ of 1.857 ± 0.013 (2*s*, $n = 4$), an expected age of 519.4 ± 6.5 Ma, and an initial Sr ratio of 0.72607 ± 0.0007 (taken from Hogmalm *et al.* 2017). For GL-O-NP, the calculated $^{87}Rb/^{86}Sr$ ratio is 33.97 ± 0.35(2*s*), using a mean $^{87}Sr/^{86}Sr$ of 0.7547 ± 0.003 (2*s*, $n = 3$), a depositional age of 99.6 ± 0.9 Ma (Selby 2009), and the expected initial $^{87}Sr/^{86}Sr$ ratio of GL-O glauconite of 0.70740 ± 0.00010 (McArthur *et al.* 2012, Rousset *et al.* 2004), which reflects the Sr isotope composition of Albian-Cenomanian palaeo-seawater. Furthermore, the $^{87}Rb/^{86}Sr$ ratio of GL-O was calculated at 35.46 ± 0.42 (2*s*) using the above values, but with the mean GL-O glauconite formation age of 95.4 Ma.

Additional constraints on $^{87}Rb/^{86}Sr$ and $^{87}Sr/^{86}Sr$ of Mica-Mg and GL-O determined via MC-ICP-MS

Mica-Mg and GL-O RMs (i.e., original powders provided by CRPG) were also analysed by isotope-dilution (ID) MC-ICP-MS to further constrain their Rb and Sr mass fractions and $^{87}Rb/^{86}Sr$ and $^{87}Sr/^{86}Sr$ isotope ratios. FK-N-NP and Mica-Fe-NP were found to be heterogenous with respect to Rb and Sr isotopic compositions, and hence were not characterised further. The measurement results are summarised in Tables 3 and 4, and listed in Table S3. The mean $^{87}Sr/^{86}Sr$ ratio acquired by ID-MC-ICP-MS for Mica-Mg is 1.8406 ± 0.0002 (2*s*, $n = 4$), and the mean ID $^{87}Rb/^{86}Sr$ ratio of Mica-Mg is 151.40 ± 0.54 (2*s*, $n = 4$). The Rb-Sr ID-MC-ICP-MS data of Mica-Mg powder yielded a model age of 525 ± 1 Ma (Figure 8) using the initial Sr ratio of 0.72607 ± 0.0007 (Hogmalm *et al.* 2017). The calculated mean age of 519.4 ± 6.5 Ma for the Bekily area is slightly younger, but within uncertainty of the ID-MC-ICP-MS age or *in situ* K-Ar age (Hogmalm *et al.* 2017, Olierook *et al.* 2020, Solé 2021), and also within the range reported recently by Jegal *et al.* (2022) (see also Table 1). In addition, the mean $^{87}Sr/^{86}Sr$ ratio acquired by ID-MC-ICP-MS for Mica-Mg is 1.8406 ± 0.0002 (2*s*, $n = 4$) which agrees, within an uncertainty of 0.7%, with the mean $^{87}Sr/^{86}Sr$ of Mica-Mg-NP (1.857 ± 0.013, 2*s*, $n = 4$) obtained in this study by LA-ICP-MS/MS. In contrast, the mean $^{87}Rb/^{86}Sr$ ratio of Mica-Mg is 151.40 ± 0.54 (2*s*, $n = 4$), which is lower than the calculated $^{87}Rb/^{86}Sr$ (i.e., 155.23 ± 2.0, see the above section) by 2.5%, and lower than the previously reported $^{87}Rb/^{86}Sr$ for Mica-Mg-NP in Hogmalm *et al.* (2017) and Olierook *et al.* (2020) by 2.1% and 3.5%, respectively (See Table 1). This variation between the $^{87}Rb/^{86}Sr$ ratios of the Mica-Mg-NP (obtained via LA-ICP-MS/MS) and the $^{87}Rb/^{86}Sr$ of the original Mica-Mg mineral powder (obtained via ID-MC-ICP-MS), in addition to

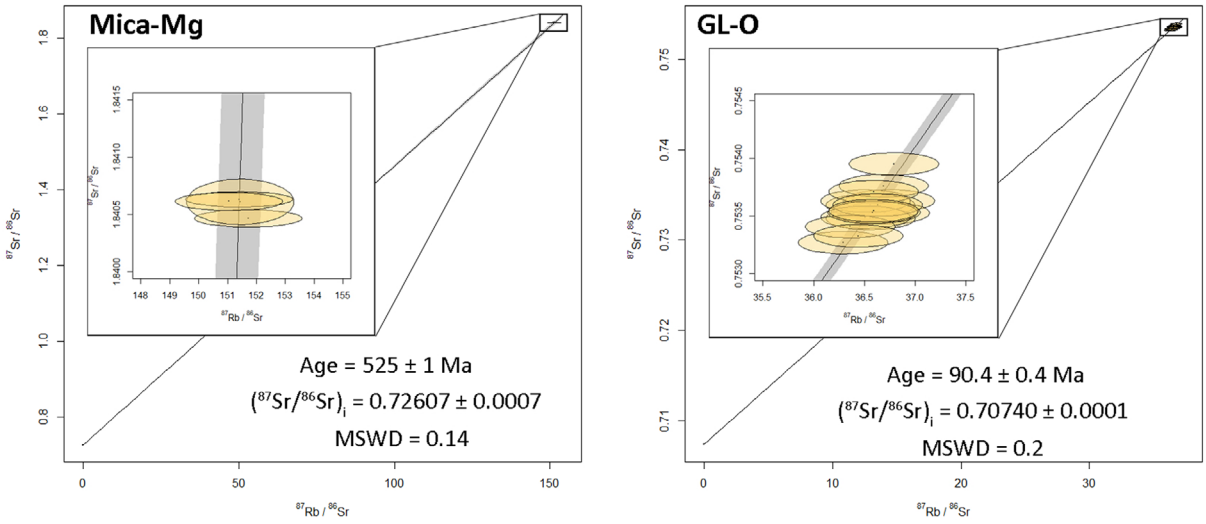

Figure 8. Rb-Sr model age of Mica-Mg (left) and GL-O (right) calculated using Rb-Sr data measured by ID MC-ICP-MS.

the variation in $^{87}Rb/^{86}Sr$ and $^{87}Sr/^{86}Sr$ reported in the literature (Jegal *et al.* 2022, Olierook *et al.* 2020, Hogmalm *et al.* 2017), indicate the necessity of future studies to better characterise multiple batches of Mica-Mg powders and produced NPs, using combinations of ID-MC-ICP-MS or ID-TIMS as well as *in situ* Rb-Sr dating approaches.

The measured solution-based (ID-MC-ICP-MS) $^{87}Rb/^{86}Sr$ and $^{87}Sr/^{86}Sr$ ratios of the GL-O powder are 36.57 ± 0.26 (2*s*, *n* = 16) and 0.753561 ± 0.00032 (2*s*, *n* = 16), respectively. The latter is in excellent agreement with the recommended $^{87}Sr/^{86}Sr$ ratio for GL-O (0.7535 ± 0.0010) based on the work of Govindaraju (1995) and also previous studies of GL-O (Odin *et al.* 1982), and slightly lower, but within uncertainty of 0.4%, with the mean $^{87}Sr/^{86}Sr$ of GL-O-NP acquired by the LA-ICP-MS/MS (0.75747 ± 0.0031) (see Figure 7b). The ID-based GL-O model Rb-Sr age is 90.4 ± 0.4 Ma (see Figure 8), which is in good agreement, within uncertainty, with the Rb-Sr age of GL-O (91.7 ± 7.1 Ma, recalculated based on data of Odin *et al.* (1982)). However, the above Rb-Sr age of GL-O is younger than the reported K-Ar age for GL-O of 95 ± 1 Ma (Odin *et al.* 1982, Smith *et al.* 1998, Fiet *et al.* 2006, Derkowski *et al.* 2009), and also younger than the expected stratigraphic age for GL-O of 99.6 ± 0.9 Ma (Selby 2009). These younger Rb-Sr and K-Ar 'bulk' ages could be related to the above-mentioned mineral impurities (apatite, calcite) within GL-O grains and thus powders, which might impact the 'bulk' glauconite age produced via ID MC-ICP-MS and K-Ar dating (Derkowski *et al.* 2009, Fiet *et al.* 2006, Odin *et al.* 1982, Smith *et al.* 1998), as both ages are systematically younger than the expected stratigraphic age for GL-O glauconite.

Assessment of nano-powder pellets as suitable reference materials

Mica-Mg-NP: Mica-Mg-NP was used as a primary RM to determine the age of GL-O grains and MDC phlogopite flakes, as well as Mica-Fe-NP. Test portions were analysed over two or three sessions using LA-ICP MS/MS, and the measurement results are presented in Table S4. Two sets of $^{87}Rb/^{86}Sr$ and $^{87}Sr/^{86}Sr$ values of Mica-Mg-NP were tested to normalise Rb-Sr data of the above samples; the first set was calculated from the assumed age of 519.4 (Hogmalm *et al.* 2017) and the second set was measured directly from Mica-Mg by MC-ICP-MS and labelled here as the age of Mica-Mg is 525 Ma (see Table 5). Overall, the obtained ages are within uncertainty with the expected ages for GL-O grains, MDC and Mica-Fe-NP (see the summary in Figure 9, and Table S6 and isochron plots (Figures S7–S12)).

The mean age of GL-O grains measured by LA-ICP-MS/MS using $^{87}Rb/^{86}Sr$ and $^{87}Sr/^{86}Sr$ values of Mica-Mg measured by MC-ICP-MS, was 99 ± 3 Ma (*n* = 3, 2*s*). When the data was calibrated using $^{87}Rb/^{86}Sr$ and $^{87}Sr/^{86}Sr$ values that assume the age of Mica-Mg-NP is 519.4 Ma, GL-O grains yielded a mean age of 101 ± 2 (*n* = 3, 2*s*). These ages were calculated by anchoring the isochron to an initial $^{87}Sr/^{86}Sr$ of 0.70740 ± 0.0001 that represents the expected Sr isotope composition of coeval

Table 5.
$^{87}Rb/^{86}Sr$ and $^{87}Sr/^{86}Sr$ reference values for Mica-Mg-NP and GL-O-NP tested in this study for Rb-Sr calibration of unknown samples

Reference material	$^{87}Rb/^{86}Sr$	2*s*	$^{87}Sr/^{86}Sr$	2*s*	Note
Mica-Mg-NP, age = 525 Ma (ID data)	151.4	0.5	1.8406	2E-04	Both $^{87}Rb/^{86}Sr$ and $^{87}Sr/^{86}Sr$ values were measured via ID-MC-ICP-MS
Mica-Mg-NP, age = 519.4 Ma*	155.27	2	1.857	0.013	$^{87}Sr/^{86}Sr$ was measured by LA-ICP-MS/MS (normalised to NIST SRM 610) and $^{87}Rb/^{86}Sr$ value was calculated assuming the age of Mica-Mg-NP at 519.4 ± 6.5 Ma.
GL-O-NP, age = 90.4 Ma (ID data)	36.57	0.3	0.7536	3E-04	Both $^{87}Rb/^{86}Sr$ and $^{87}Sr/^{86}Sr$ values were measured via ID-MC-ICP-MS
GL-O-NP, age = 95.4 Ma*	35.46	0.4	0.7547	0.003	$^{87}Sr/^{86}Sr$ was measured by LA-ICP-MS/MS (normalised to NIST SRM 610) and $^{87}Rb/^{86}Sr$ value was calculated assuming the age of GL-O-NP at 95.4 ± 2.3 Ma.
GL-O-NP, age = 99.6 Ma	33.97	0.4	0.7547	0.003	$^{87}Sr/^{86}Sr$ was measured by LA-ICP-MS/MS (normalised to NIST SRM 610) and $^{87}Rb/^{86}Sr$ value was calculated assuming the age of GL-O-NP at 99.6 ± 0.9Ma.

* Preferred values

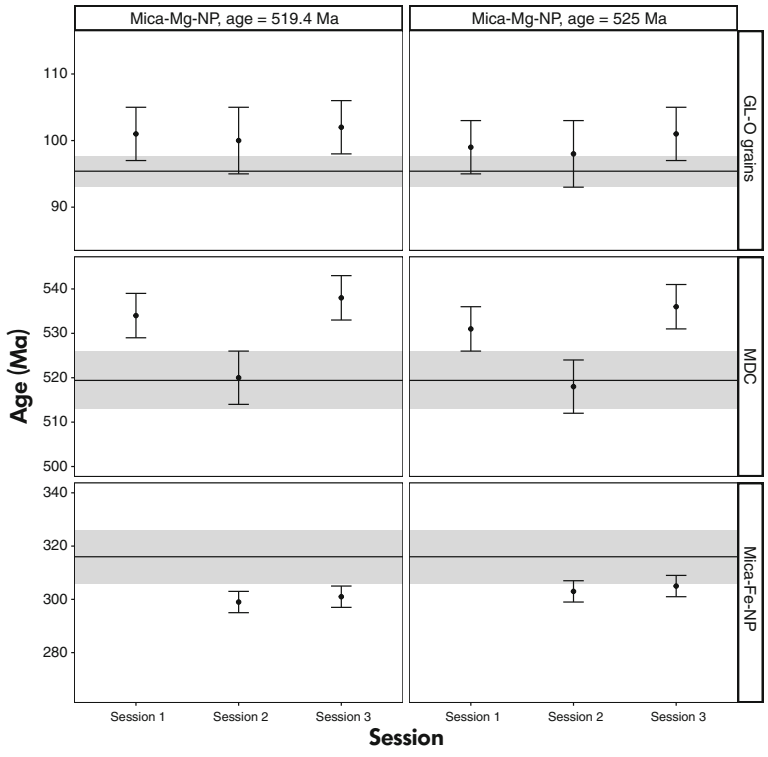

Figure 9. A summary plot showing calculated Rb-Sr ages of MDC phlogopite, GL-O glauconite grains and Mica-Fe-NP biotite (see Table S6 in online supporting information), derived from *in situ*-derived Rb-Sr isochrons based on measured $^{87}Rb/^{86}Sr$ and $^{87}Sr/^{86}Sr$ data calibrated using Mica-Mg-NP with two sets of $^{87}Rb/^{86}Sr$ and $^{87}Sr/^{86}Sr$ values; one calculated via LA-ICP-MS and the age of 519.4 Ma (labelled as Mica-Mg-NP, 519.4 Ma) and the other set of $^{87}Rb/^{86}Sr$ and $^{87}Sr/^{86}Sr$ constrained by ID MC-ICP-MS (labelled as Mica-Mg-NP, age = 525 Ma). Labels in the right side rectangles refer to the sample/mineral name. The black horizontal line and grey box represent the expected/published age with the associated uncertainty (2*s*) for GL-O grains (95.4 ± 7.8 Ma, the mean of Ka-Ar and Rb-Sr ages and the depositional age (Odin *et al.* 1982, Derkowski *et al.* 2009, Selby 2009)), MDC (519.4 ± 6.5 Ma, Redaa *et al.* (2021)) and Mica-Fe-NP (316 ± 9 Ma, Zimmermann *et al.* (1985)).

seawater (McArthur *et al.* 2012; see Figures S8 and S11). The above ages (99 ± 3 Ma and 101 ± 2 Ma) are overlapping, and they also overlap with the depositional age of GL-O grains (99.6 ± 0.9 Ma, Selby (2009)). However, these ages are older than the Rb-Sr and K-Ar ages of 'bulk' GL-O constrained at 91.7 ± 7.1 Ma (recalculated from Odin *et al.* (1982)) and 94 ± 1 Ma (Solé 2021), respectively. This could be related to matrix effects between GL-O grains and Mica-Mg-NP (i.e., differences in chemical and ablation properties), as this effect could impact the accuracy of the *in situ* Rb-Sr age by up to 8% (Redaa *et al.* 2021). Here, the obtained ages of GL-O are within 5% of the expected mean age of GL-O (95.4 ± 2.3 Ma). Therefore, it is necessary to further constrain the age of 'pure' glauconite grains of GL-O by ID methods via either MC-ICP-MS or TIMS to accurately constrain the age of pristine GL-O glauconite, and to confirm whether the above age is the actual depositional age, or if it was biased due to the matrix effects. Currently, GL-O grains can be used as a secondary RM for *in situ* Rb-Sr dating of glauconite when Mica-Mg-NP is used as a primary RM, with a reference age of 95.4 ± 2.3 Ma that represents the mean GL-O age as discussed above.

The *in situ* Rb-Sr ages for MDC were calculated by anchoring the isochrons to an initial $^{87}Sr/^{86}Sr$ ratio of 0.72607 ± 0.0007 (Hogmalm *et al.* 2017, see isochron plots in Figures S7 and S10). MDC yielded ages of 534 ± 5 Ma, 520 ± 6 Ma, and 538 ± 5 Ma for sessions 1, 2 and 3, respectively (with Rb-Sr data of MDC normalised to Mica-Mg-NP with an assumed age of 519.4 Ma; see Figure 9). Using $^{87}Rb/^{86}Sr$ and $^{87}Sr/^{86}Sr$ values measured via MC-ICP-MS for Mica-Mg produced younger ages by ~0.5%. Although the calculated ages in session 1 and 3 are older than the expected age of 519.4 ± 6.5 Ma (Hogmalm *et al.* 2017), they are within the laboratory's (long-term) intermediate measurement precision of ±3%. The possible reasons for the biases in the above Rb-Sr ages of MDC are mainly related to matrix effects, coupled with possible internal heterogeneity in Mica-Mg-NP (see detailed discussion in Redaa *et al.* (2021).

Mica-Fe-NP ages were calculated by anchoring the Rb-Sr isochrons to 0.709797 ± 0.016, which was constrained by Turpin *et al.* (1990) (see Figures S9 and S12). When the sample was calibrated to Mica-Mg-NP (with assumed age of 519.4 Ma) the calculated ages were 299 ± 4 Ma and 301 ± 4 Ma, for session 2 and 3, respectively (see Figure 9). Calibrating the data using ID Rb-Sr values for Mica-Mg (Table 5) produced ages of 303 ± 4 Ma and 305 ± 4 Ma for sessions 2 and 3, respectively. These ages overlap the previously reported *in situ* Rb-Sr age for Mica-Fe as 303.3 ± 1.9 Ma (Rösel and Zack 2022). However, these *in situ* Rb-Sr ages are slightly younger than the previously reported Rb-Sr age for Mica-Fe (316 ± 10 Ma) (Govindaraju 1979). This bias suggests matrix effects between Mica-Mg-NP and Mica-Fe-NP.

In summary, Mica-Mg-NP can be used as a RM to calibrate *in situ* Rb-Sr data of phlogopite, glauconite and biotite by LA-ICP-MS/MS using the recommended reference age of 519.4 Ma. However, further characterisation of secondary RMs for these minerals are needed to better constrain the possible impacts of the matrix effects.

GL-O-NP: GL-O-NP was also used as a primary RM to normalise $^{87}Rb/^{86}Sr$ and $^{87}Sr/^{86}Sr$ data and to calculate the Rb-Sr age of GL-O grains, MDC and Mica-Fe-NP (see Figures S13–S21). These materials were analysed over two or three sessions, and the measurement results are presented in Table S5, and summarised in Figure 10. Three different sets of $^{87}Rb/^{86}Sr$ and $^{87}Sr/^{86}Sr$ data were obtained from the plausible reference ages for GL-O-NP (see Table 5). The first set was obtained via the ID-MC-ICP-MS data and labelled here with an age of 90.4 Ma, whereas the other two sets were constrained by the LA-ICP-MS/MS data, assuming different ages for GL-O (95.4 Ma = K-Ar age; and 99 Ma = expected depositional age) as described in the above section. The calculated ages for GL-O grains and MDC showed negligible variation (< 0.5%) between the sessions (see Figure 10). However, Mica-Fe-NP was more variable (3.5% RSD), which suggests the presence of matrix effects between GL-O-NP and Mica-Fe-NP.

When MDC was calibrated against GL-O-NP (with the assumed age of 99.6 Ma, Table 5), the calculated age was within 1.5% of the expected age of 519.4 ± 6.5 Ma for all three measurement sessions, i.e., 528 ± 5 Ma, 527 ± 6 Ma, and 524 ± 5 Ma, respectively (Figure 10). In contrast, MDC ages become younger than the expected age by ~ 3% and ~ 6% when the data was normalised to GL-O-NP with the assumed ages of 95.4 Ma, and to ID-MC-ICP-MS Rb-Sr values of GL-O, respectively (Figure 10).

The *in situ* Rb-Sr ages of GL-O grains showed also systematic variation when the $^{87}Rb/^{86}Sr$ and $^{87}Sr/^{86}Sr$ data of the sample were calibrated using the different reference values of GL-O-NP (Table 5). Noticeably, GL-O grains yielded older ages when the Rb-Sr data was normalised to GL-O-NP assuming its age at 99.6 Ma (see Table 5), and the ages being younger by 5% and 8.3% when the data was normalised to GL-O-NP with the assumed age of 95.4 Ma, and to ID-MC-ICP-MS Rb-Sr values of GL-O, respectively (Figure 10).

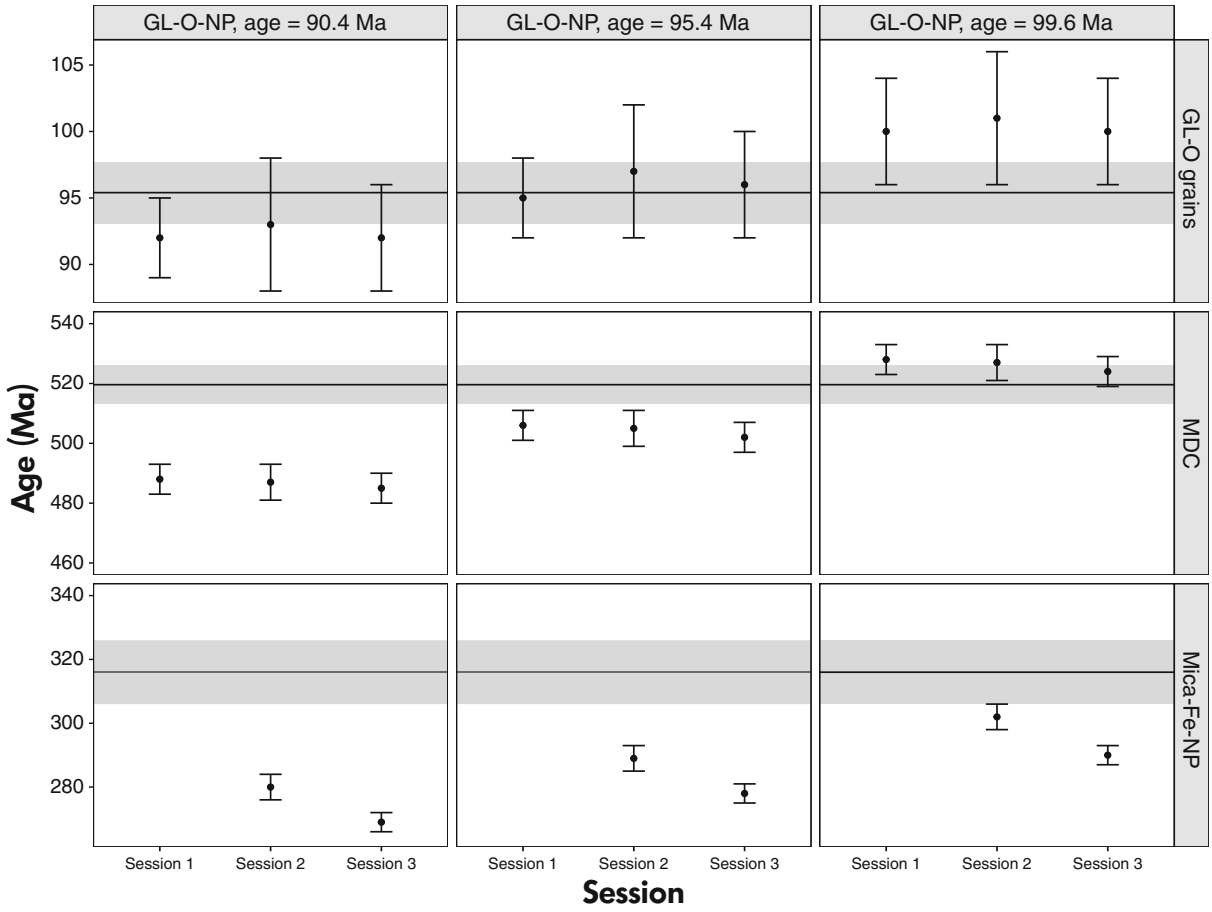

Figure 10. A summary plot showing calculated Rb-Sr ages of MDC phlogopite and Mica-Fe-NP biotite (see Table S6 in online supporting information), derived from *in situ*-derived Rb-Sr isochrons based on measured $^{87}Rb/^{86}Sr$ and $^{87}Sr/^{86}Sr$ data calibrated using GL-O-NP with different sets of calibration $^{87}Rb/^{86}Sr$ and $^{87}Sr/^{86}Sr$ values. "GL-O-NP, age = 95 Ma" and "GL-O-NP, age = 99.6 Ma" refer to that the $^{87}Rb/^{86}Sr$ data of the samples (MDC and Mica-Fe-NP) were calibrated to GL-O-NP with assumed ages at 95 Ma and 99.6 Ma, respectively, whereas $^{87}Sr/^{86}Sr$ of GL-O-NP was measured by LA-ICP-MS and normalised to NIST SRM 610. "GL-O-NP, age = 90.4 Ma" indicates that the ages were obtained by calibrating $^{87}Rb/^{86}Sr$ and $^{87}Sr/^{86}Sr$ of the samples (MDC and Mica-Fe-NP) using $^{87}Rb/^{86}Sr$ and $^{87}Sr/^{86}Sr$ of GL-O acquired by the MC-ICP-MS. The black horizontal line and grey box represents, the expected/published age with the associated uncertainty (2*s*) (see also references in Table 1).

When the $^{87}Rb/^{86}Sr$ and $^{87}Sr/^{86}Sr$ data of Mica-Fe-NP was calibrated to GL-O-NP (with an assumed age of 99.6 Ma), the sample yielded an age in session 2 of 302 ± 4 Ma, which overlaps with the previously reported K-Ar age. However, the produced *in situ* Rb-Sr age for Mica-Fe-NP from session 3 (290 ± 3 Ma) is younger than the expected age by about 6%. Moreover, using the other previously discussed $^{87}Rb/^{86}Sr$ and $^{87}Sr/^{86}Sr$ values of GL-O-NP (i.e., constrained via ID MC-ICP-MS or assuming an age of 95.4 Ma) for calibration, Mica-Fe-NP data yielded ages that are younger than the expected age by more than 10% (see Figure 10 and Table S6).

The above results indicate that GL-O-NP could be a suitable RM for *in situ* Rb-Sr dating by LA-ICP-MS/MS, considering its homogeneity. We recommend using $^{87}Rb/^{86}Sr$ and $^{87}Sr/^{86}Sr$ reference values for GL-O-NP calculated assuming the mean reported age of 95.4 Ma (see Table 5) Further, we recommend that $^{87}Rb/^{86}Sr$ and $^{87}Sr/^{86}Sr$ ratios of each GL-O-NP pellet need to be constrained independently by measuring its $^{87}Sr/^{86}Sr$, then calculating the $^{87}Rb/^{86}Sr$ using the age of 95.4 Ma, and the initial Sr ratio of 0.70740 ± 0.00010 (Rousset *et al.* 2004, McArthur *et al.* 2012) following the approach described in Hogmalm *et al.* (2017).

Conclusions

Nano-powder pellets of four silicate mineral reference materials (GL-O glauconite, Mica-Mg phlogopite, Mica-Fe biotite and FK-N feldspar) were tested for *in situ* Rb-Sr dating by LA-ICP-MS/MS, and new Rb-Sr ages are presented for GL-O and Mica-Mg powders measured by ID-MC-ICP-MS.

Mica-Mg-NP and GL-O-NP are homogeneous with respect to Rb and Sr mass fractions and isotope compositions at the micro-scale level, and these NP materials can be used as reliable RMs for *in situ* Rb-Sr dating for phlogopite, glauconite, and biotite. We recommend using 519.4 ± 6.5 Ma and 95.4 ± 2.3 Ma as the reference ages for Mica-Mg-NP and GL-O-NP respectively. It is recommended for laboratories to constrain the Rb-Sr isotopic composition of Mica-Mg-NP and GL-O-NP by measuring $^{87}Sr/^{86}Sr$ over multiple sessions normalised to NIST SRM 610 glass, then calculate the working $^{87}Rb/^{86}Sr$ value using the above ages following the approach described in Hogmalm *et al.* (2017). Future work, including additional high-precision Rb-Sr dating of different NP batches by ID-TIMS or MC-ICP-MS is needed to further constrain Rb-Sr isotopic compositions of these RMs, allowing for further expansion and improvement of the use of mineral-specific NP-based RMs for *in situ* Rb-Sr dating applications via LA-ICP-MS/MS and/or multi-collector LA-MC-ICP-MS/MS techniques.

Acknowledgements

This work was primarily supported by the Australian Research Council under the ARC Discovery Project (DP210100462) "Glauconite: Archive recording timing and triggers of Cambrian radiation", and partly supported by Agilent Technologies. The work was also supported by the Mineral Exploration Cooperative Research Centre (MinEx CRC) whose activites are funded by the Australian Governmnet's Cooperative Research Centre Programme. This is MinEx CRC Document 2022/84. We also acknowledge assistance with analytical work on selected RMs by Wei Hong from the University of Adelaide. Additional thanks go to the iolite team, specifically to Bence Paul and Joe Petrus, for providing a free licence and support for iolite4 software. Mr Ken Neubauer from Adelaide Microscopy is also acknowledged for the assistance with the SEM analysis and imaging of mineral reference materials and fused glasses. Finally, we would also like to thank the editor of GGR and three anonymous reviewers for their constructive comments and feedback, which improved the overall quality of this work. Open access publishing facilitated by The University of Adelaide, as part of the Wiley - The University of Adelaide agreement via the Council of Australian University Librarians.

Funding Statement

Open access publishing facilitated by The University of Adelaide, as part of the Wiley - The University of Adelaide agreement via the Council of Australian University Librarians.

Data availability statement

The data supporting the findings of this study are available within the article and its supplementary materials.

References

Agatemor C. and Beauchemin D. (2011)
Matrix effects in inductively coupled plasma-mass spectrometry: A review. **Analytica Chimica Acta**, **706**, 66–83.

Armistead S.E., Collins A.S., Redaa A., Jepson G., Gillespie J., Gilbert S., Blades M.L., Foden J.D. and Razakamanana T. (2020)
Structural evolution and medium-temperature thermochronology of central Madagascar: Implications for Gondwana amalgamation. **Journal of the Geological Society**, **177**, 784–798.

Awaji S., Nakamura K., Nozaki T. and Kato Y. (2006)
A simple method for precise determination of 23 trace elements in granitic rocks by ICP-MS after lithium tetraborate fusion. **Resource Geology**, **56**, 471–478.

Bevan D., Coath C.D., Lewis J., Schwieters J., Lloyd N., Craig G., Wehrs H. and Elliott T. (2021)
In situ Rb-Sr dating by collision cell, multicollection inductively coupled plasma-mass spectrometry with pre-cell mass-filter (CC-MC-ICP-MS/MS). **Journal of Analytical Atomic Spectrometry**, **36**, 917–931.

Boulesteix T., Solé J., Pi T. and Cathelineau M. (2020)
Reappraisal of the GL-O reference material for K-Ar dating: New insight from microanalysis, single-grain and milligram Ar measurements. **Geostandards and Geoanalytical Research**, **44**, 287–306.

Dalton H., Giuliani A., Phillips D., Hergt J., Maas R., Matchan E., Woodhead J. and O'Brien H. (2020)
A comparison of geochronological methods commonly applied to kimberlites and related rocks: Three case studies from Finland. **Chemical Geology**, **558**, 119899.

references

Derkowski A., Środoń J., Franus W., Uhlík P., BanaŚ M., Zieliński G., ČaploviČová M. and Franus M. (2009)
Partial dissolution of glauconitic samples: Implications for the methodology of K-Ar and Rb-Sr dating. **Clays and Clay Minerals**, **57**, 531–554.

Eggins S.M. (2003)
Laser ablation ICP-MS analysis of geological materials prepared as lithium borate glasses. **Geostandards Newsletter: The Journal of Geostandards and Geoanalysis**, **27**, 147–162.

Elburg M., Vroon P., van der Wagt B. and Tchalikian A. (2005)
Sr and Pb isotopic composition of five USGS glasses (BHVO-2G, BIR-1G, BCR-2G, TB-1G, NKT-1G). **Chemical Geology**, **223**, 196–207.

Fedorowich J.S., Richards J.P., Jain J.C., Kerrich R. and Fan J. (1993)
A rapid method for REE and trace-element analysis using laser sampling ICP-MS on direct fusion whole-rock glasses. **Chemical Geology**, **106**, 229–249.

Fiet N., Quidelleur X., Parize O., Bulot L.G. and Gillot P.Y. (2006)
Lower Cretaceous stage durations combining radiometric data and orbital chronology: Towards a more stable relative time scale? **Earth and Planetary Science Letters**, **246**, 407–417.

Fiorentini M.L., O'Neill C., Giuliani A., Choi E., Maas R., Pirajno F. and Foley S. (2020)
Bushveld superplume drove Proterozoic magmatism and metallogenesis in Australia. **Scientific reports**, **10**, 1–10.

Forster M.A., Lister G.S. and Lennox P.G. (2014)
Dating deformation using crushed alkali feldspar: $^{40}Ar/^{39}Ar$ geochronology of shear zones in the Wyangala Batholith, NSW, Australia. **Australian Journal of Earth Sciences**, **61**, 619–629.

Garbe-Schönberg D. and Müller S. (2014)
Nano-particulate pressed powder tablets for LA-ICP-MS. **Journal of Analytical Atomic Spectrometry**, **29**, 990–1000.

Gardien V., Thompson A.B., Grujic D. and Ulmer P. (1995)
Experimental melting of biotite + plagioclase + quartz ± muscovite assemblages and implications for crustal melting. **Journal of Geophysical Research: Solid Earth**, **100**, 15581–15591.

Gilbert S., Danyushevsky L., Robinson P., Wohlgemuth-Ueberwasser C., Pearson N., Savard D., Norman M. and Hanley J. (2013)
A comparative study of five reference materials and the Lombard Meteorite for the determination of the platinum-group elements and gold by LA-ICP-MS. **Geostandards and Geoanalytical Research**, **37**, 51–64.

Gilbert S.E., Danyushevsky L.V., Goemann K. and Death D. (2014)
Fractionation of sulphur relative to iron during laser ablation-ICP-MS analyses of sulphide minerals: Implications for quantification. **Journal of Analytical Atomic Spectrometry**, **29**, 1024–1033.

Gorojovsky L. and Alard O. (2020)
Optimisation of laser and mass spectrometer parameters for the *in situ* analysis of Rb/Sr ratios by LA-ICP-MS/MS. **Journal of Analytical Atomic Spectrometry**, **35**, 2322–2336.

Govindaraju K. (1979)
Report (1968–1978) on two mica reference samples: Biotite Mica-Fe and Phlogopite Mica-Mg. **Geostandards Newsletter**, **3**, 3–24.

Govindaraju K. (1984)
Report (1973–1984) on two ANRT geochemical reference samples: Granite GS-N and Potash Feldspar FK-N. **Geostandards Newsletter**, **8**, 173–206.

Govindaraju K. (1994)
1994 compilation of working values and sample description for 383 geostandards. **Geostandards Newsletter**, **18 (Special Issue)**, 158pp.

Govindaraju K. (1995)
1995 working values with confidence limits for twenty-six CRPG, ANRT and IWG-GIT geostandards. **Geostandards Newsletter**, **19 (Special Issue)**, 32pp.

Govindaraju K. and Roelandts I. (1988)
Compilation report (1966–1987) on trace elements in five CRPG geochemical reference samples: Basalt BR; Granites, GA and GH; Micas, Biotite Mica-Fe and Phlogopite Mica-Mg. **Geostandards Newsletter**, **12**, 119–201.

Gray T. (2009)
Elements: A visual exploration of every known atom in the universe. **Black Dog and Leventhal Publishers, Inc. (New York)**.

Grove M. and Harrison T.M. (1996)
$^{40}Ar^*$ diffusion in Fe-rich biotite. **American Mineralogist**, **81**, 940–951.

He Z., Huang F., Yu H., Xiao Y., Wang F., Li Q., Xia Y. and Zhang X. (2016)
A flux-free fusion technique for rapid determination of major and trace elements in silicate rocks by LA-ICP-MS. **Geostandards and Geoanalytical Research**, **40**, 5–21.

Hogmalm K.J., Zack T., Karlsson A.K.O., Sjöqvist A.S.L. and Garbe-Schönberg D. (2017)
In situ Rb-Sr and K-Ca dating by LA-ICP-MS/MS: An evaluation of N_2O and SF_6 as reaction gases. **Journal of Analytical Atomic Spectrometry**, **32**, 305–313.

Hu Z., Gao S., Liu Y., Hu S., Chen H. and Yuan H. (2008)
Signal enhancement in laser ablation ICP-MS by addition of nitrogen in the central channel gas. **Journal of Analytical Atomic Spectrometry**, **23**, 1093–1101.

Jegal Y., Zimmermann C., Reisberg L., Yeghicheyan D., Cloquet C., Peiffert C., Gerardin M., Deloule E. and Mercadier J. (2022)
Characterisation of reference materials for *in situ* Rb-Sr dating by LA-ICP-MS/MS. **Geostandards and Geoanalytical Research**. https://doi.org/10.1111/ggr.12456

references

Jochum K.P., Stoll B., Herwig K., Willbold M., Hofmann A.W., Amini M., Aarburg S., Abouchami W., Hellebrand E., Mocek B., Raczek I., Stracke A., Alard O., Bouman C., Becker S., Dücking M., Brätz H., Klemd R., de Bruin D., Canil D., Cornell D., de Hoog C.-J., Dalpé C., Danyushevsky L., Eisenhauer A., Gao Y., Snow J.E., Groschopf N., Günther D., Latkoczy C., Guillong M., Hauri E.H., Höfer H.E., Lahaye Y., Horz K., Jacob D.E., Kasemann S.A., Kent A.J.R., Ludwig T., Zack T., Mason P.R.D., Meixner A., Rosner M., Misawa K., Nash B.P., Pfänder J., Premo W.R., Sun W.D., Tiepolo M., Vannucci R., Vennemann T., Wayne D. and Woodhead J.D. (2006)
MPI-DING reference glasses for *in situ* microanalysis: New reference values for element concentrations and isotope ratios. Geochemistry Geophysics Geosystems, 7.

Langmuir C.H., Vocke R.D., Hanson G.N. and Hart S.R. (1978)
A general mixing equation with applications to Icelandic basalts. Earth and Planetary Science Letters, 37, 380–392.

Laureijs C.T., Coogan L.A. and Spence J. (2021)
In-situ Rb-Sr dating of celadonite from altered upper oceanic crust using laser ablation ICP-MS/MS. Chemical Geology, 579, 120339.

Li S.-S., Santosh M., Farkaš J., Redaa A., Ganguly S., Kim S.W., Zhang C., Gilbert S. and Zack T. (2020)
Coupled U-Pb and Rb-Sr laser ablation geochronology trace Archean to Proterozoic crustal evolution in the Dharwar Craton, India. Precambrian Research, 343, 105709.

Lin J., Liu Y., Yang Y. and Hu Z. (2016)
Calibration and correction of LA-ICP-MS and LA-MC-ICP-MS analyses for element contents and isotopic ratios. Solid Earth Sciences, 1, 5–27.

Maas R., Grew E.S. and Carson C.J. (2015)
Isotopic constraints (Pb, Rb-Sr, Sm-Nd) on the sources of early Cambrian pegmatites with boron and beryllium minerals in the Larsemann Hills, Prydz Bay, Antarctica. The Canadian Mineralogist, 53, 249–272.

McArthur J., Howarth R. and Shields G. (2012)
Strontium isotope stratigraphy. In: Gradstein F.M., Ogg J.G., Schmitz M.D. and Ogg G.M. (eds), The geologic time scale. Elsevier, 127–144.

McArthur J., Rio D., Massari F., Castradori D., Bailey T., Thirlwall M. and Houghton S. (2006)
A revised Pliocene record for marine-$^{87}Sr/^{86}Sr$ used to date an interglacial event recorded in the Cockburn Island Formation, Antarctic Peninsula. Palaeogeography, Palaeoclimatology, Palaeoecology, 242, 126–136.

Nebel O. and Mezger K. (2006)
Reassessment of the NBS SRM-607 K-feldspar as a high precision Rb/Sr and Sr isotope reference. Chemical Geology, 233, 337–345.

Miliszkiewicz N., Walas S. and Tobiasz A. (2015)
Current approaches to calibration of LA-ICP-MS analysis. Journal of Analytical Atomic Spectrometry, 30, 327–338.

O'Connor C., Landon M.R. and Sharp B.L. (2007)
Absorption coefficient modified pressed powders for calibration of laser ablation inductively coupled plasma-mass spectrometry. Journal of Analytical Atomic Spectrometry, 22, 273–282.

Odin G. (1976)
Glauconite GL-O, interlaboratory standard for radiochronometric analysis. Analusis, 4, 287–291.

Odin G.S., Adams C.J., Armstrong R.L., Bagdasaryan G.P., Baksi A.K., Balogh K., Barnes I.L., Boelrijk N.A.I.M., Bonadonna F.P., Bonhomme M.G., Cassignol C., Chanin L., Gillot P.Y., Gledhill A., Govindaraju K., Harakal R., Warre W., Hebeda E.H., Hunziker J.C., Ingamells C.O., Kawashita K., Kiss E., Kreuzer H., Long L.E., McDougall I., McDowell F., Mehnert H., Montigny R., Pasteels P., Radicati F., Rex D.C., Rundle C.C., Savelli C., Sonet J., Weline E. and Zimmermann J.L. (1982)
Interlaboratory standards for dating purposes. In: Odin G.S. (ed.), Numerical dating in stratigraphy. Wiley (Chichester), 123–148.

Olierook H.K., Rankenburg K., Ulrich S., Kirkland C.L., Evans N.J., Brown S., McInnes B.I., Prent A., Gillespie J. and McDonald B. (2020)
Resolving multiple geological events using *in situ* Rb-Sr geochronology: Implications for metallogenesis at Tropicana, Western Australia. Geochronology, 2, 283–303.

Paton C., Hellstrom J., Paul B., Woodhead J. and Hergt J. (2011)
Iolite: Freeware for the visualisation and processing of mass spectrometric data. Journal of Analytical Atomic Spectrometry, 26, 2508–2518.

Phillips D., Matchan E., Honda M. and Kuiper K. (2017)
Astronomical calibration of $^{40}Ar/^{39}Ar$ reference minerals using high-precision, multi-collector (ARGUSVI) mass spectrometry. Geochimica et Cosmochimica Acta, 196, 351–369.

Pin C. and Bassin C. (1992)
Evaluation of a strontium-specific extraction chromatographic method for isotopic analysis in geological materials. Analytica Chimica Acta, 269, 249–255.

Rafiei M., Löhr S., Baldermann A., Webster R. and Kong C. (2020)
Quantitative petrographic differentiation of detrital vs diagenetic clay minerals in marine sedimentary sequences: Implications for the rise of biotic soils. Precambrian Research, 350, 105948.

Redaa A., Farkaš J., Gilbert S., Collins A.S., Wade B., Löhr S., Zack T. and Garbe-Schönberg D. (2021)
Assessment of elemental fractionation and matrix effects during *in-situ* Rb-Sr dating of phlogopite by LA-ICP-MS/MS: Implications for the accuracy and precision of mineral ages. Journal of Analytical Atomic Spectrometry, 322–344.

references

Redaa A., Farkaš J., Hassan A., Collins A.S., Gilbert S. and Löhr S.C. (2022)
Constraints from *in-situ* Rb-Sr dating on the timing of tectono-thermal events in the Umm Farwah shear zone and associated Cu-Au mineralisation in the southern Arabian Shield, Saudi Arabia. Journal of Asian Earth Sciences, 224, 105037.

Rösel D. and Zack T. (2022)
LA-ICP-MS/MS single-spot Rb-Sr dating. Geostandards and Geoanalytical Research, 46, 143–168.

Rosman K. and Taylor P. (1999)
Table of isotopic masses and natural abundances. Pure and Applied Chemistry, 71, 1593–1607.

Rousset D., Leclerc S., Clauer N., Lancelot J.l., Cathelineau M. and Aranyossy J.-F.o. (2004)
Age and origin of Albian glauconites and associated clay minerals inferred from a detailed geochemical analysis. Journal of Sedimentary research, 74, 631–642.

Scheiblhofer E., Moser U., Löhr S., Wilmsen M., Farkaš J., Gallhofer D., Bäckström A.M., Zack T. and Baldermann A. (2022)
Revisiting glauconite geochronology: Lessons learned from *in situ* radiometric dating of a glauconite-rich Cretaceous shelfal sequence. Minerals, 12, 818.

Selby D. (2009)
U-Pb zircon geochronology of the Aptian/Albian boundary implies that the GL-O international glauconite standard is anomalously young. Cretaceous Research, 30, 1263–1267.

Şengün F., Bertrandsson Erlandsson V., Hogmalm J. and Zack T. (2019)
In situ Rb-Sr dating of K-bearing minerals from the orogenic Akçaabat gold deposit in the Menderes Massif, western Anatolia, Turkey. Journal of Asian Earth Sciences, 185, 104048.

Smith P.E., Evensen N.M., York D. and Odin G.S. (1998)
Single-grain ^{40}Ar-^{39}Ar ages of glauconies: Implications for the geologic time scale and global sea level variations. Science, 279, 1517–1519.

Solé J. (2021)
An automated system for measuring *in situ* K-Ar ages. Geostandards and Geoanalytical Research, 45, 659–678.

Subarkah D., Blades M.L., Collins A.S., Farkaš J., Gilbert S., Löhr S.C., Redaa A., Cassidy E. and Zack T. (2021)
Unraveling the histories of Proterozoic shales through *in situ* Rb-Sr dating and trace element laser ablation analysis. Geology, In press.

Sylvester P. (2008)
Matrix effects in laser ablation ICP-MS. In: Sylvester P.J. (ed.), Laser ablation ICP-MS in the Earth sciences: Current practices and outstanding issues. Mineralogical Association of Canada, 40, 67–78.

Tabersky D., Luechinger N.A., Rossier M., Reusser E., Hametner K., Aeschlimann B., Frick D.A., Halim S.C., Thompson J., Danyushevsky L. and Günther D. (2014)
Development and characterization of custom-engineered and compacted nanoparticles as calibration materials for quantification using LA-ICP-MS. Journal of Analytical Atomic Spectrometry, 29, 955–962.

Tillberg M., Drake H., Zack T., Hogmalm J. and Åström M. (2017)
In situ Rb-Sr dating of fine-grained vein mineralizations using LA-ICP-MS. Procedia Earth and Planetary Science, 17, 464–467.

Tillberg M., Drake H., Zack T., Kooijman E., Whitehouse M.J. and Åström M.E. (2020)
In situ Rb-Sr dating of slickenfibres in deep crystalline basement faults. Scientific Reports, 10, 1–13.

Turpin L., Cuney M., Friedrich M., Bouchez J.-L. and Aubertin M. (1990)
Meta-igneous origin of Hercynian peraluminous granites in N.W. French Massif Central: Implications for crustal history reconstructions. Contributions to Mineralogy and Petrology, 104, 163–172.

Veizer J., Ala D., Azmy K., Bruckschen P., Buhl D., Bruhn F., Carden G.A.F., Diener A., Ebneth S., Godderis Y., Jasper T., Korte C., Pawellek F., Podlaha O.G. and Strauss H. (1999)
$^{87}Sr/^{86}Sr$, $\delta^{13}C$ and $\delta^{18}O$ evolution of Phanerozoic seawater. Chemical Geology, 161, 59–88.

Vermeesch P. (2018)
IsoplotR: A free and open toolbox for geochronology. Geoscience Frontiers, 9, 1479–1493.

Villa I.M., De Bièvre P., Holden N.E. and Renne P.R. (2015)
IUPAC-IUGS recommendation on the half life of ^{87}Rb. Geochimica et Cosmochimica Acta, 164, 382–385.

Waight T., Baker J. and Willigers B. (2002)
Rb isotope dilution analyses by MC-ICP-MS using Zr to correct for mass fractionation: towards improved Rb-Sr geochronology? Chemical Geology, 186, 99–116.

Woodhead J.D. and Hergt J.M. (2001)
Strontium, neodymium and lead isotope analyses of NIST glass certified reference materials: SRM 610, 612, 614. Geostandards Newsletter: The Journal of Geostandards and Geoanalysis, 25, 261–266.

York D., Evensen N.M., Martínez M.L. and Delgado J.D.B. (2004)
Unified equations for the slope, intercept, and standard errors of the best straight line. American Journal of Physics, 72, 367–375.

Yu Z., Norman M.D. and Robinson P. (2003)
Major and trace element analysis of silicate rocks by XRF and laser ablation ICP-MS using lithium borate fused glasses: Matrix effects, instrument response and results for international reference materials. Geostandards Newsletter: The Journal of Geostandards and Geoanalysis, 27, 67–89.

references

Zack T. and Hogmalm K.J. (2016)
Laser ablation Rb/Sr dating by online chemical separation of Rb and Sr in an oxygen-filled reaction cell. Chemical Geology, 437, 120–133.

Zhang S., He M., Yin Z., Zhu E., Hang W. and Huang B. (2016)
Elemental fractionation and matrix effects in laser sampling based spectrometry. Journal of Analytical Atomic Spectrometry, 31, 358–382.

Zimmermann J., Vernet M., Guyetand G. and Dautel D. (1985)
Données sur potassium et argon (de 1976 à 1984) dans quelques échantillons géochimiques de référence. Geostandards Newsletter, 9, 205–208.

Supporting information

The following supporting information may be found in the online version of this article:

Figure S1. SEM images and elemental maps of Mica-Mg-G1.

Figure S2. SEM images and elemental maps of Mica-Fe glasses (G1 and G2).

Figure S3. SEM images and elemental maps of FK-N glasses (G1 and G2).

Figure S4. SEM images and elemental maps of GL-O-G1 glass.

Figure S5. SEM images and elemental maps of GL-O-G2 glass.

Figure S6. SEM and Nanomin images show the glauconite grains of GL-O RM with inclusions of apatite and plagioclase.

Figure S7. Isochron diagrams and calculated *in situ* Rb-Sr ages of MDC (natural phlogopite). Data were acquired by LA-ICP-MS/MS and normalised using Mica-Mg-NP (with assumed age of 519.6 Ma) over three measurement sessions.

Figure S8. Isochron diagrams and calculated *in situ* Rb-Sr ages of GL-O (natural glauconite grains). Data were acquired by LA-ICP-MS/MS and normalised using Mica-Mg-NP (with assumed age of 519.6 Ma) over three measurement sessions.

Figure S9. Isochron diagrams and calculated *in situ* Rb-Sr ages of Mica-Fe-NP (biotite). Data were acquired by LA-ICP-MS/MS and normalised using Mica-Mg-NP (with assumed age of 519.6 Ma) over two measurement sessions.

Figure S10. Isochron diagrams and calculated *in situ* Rb-Sr ages of MDC (natural phlogopite). Data were acquired by LA-ICP-MS/MS and normalised using Mica-Mg-NP (with Rb-Sr values acquired via MC-ICP-MS) over three measurement sessions.

Figure S11. Isochron diagrams and calculated *in situ* Rb-Sr ages of GL-O (natural glauconite grains). Data were acquired by LA-ICP-MS/MS and normalised using Mica-Mg-NP (with Rb-Sr values acquired via MC-ICP-MS) over three measurement sessions.

Figure S12. Isochron diagrams and calculated *in situ* Rb-Sr ages of Mica-Fe-NP (biotite). Data were acquired by LA-ICP-MS/MS and normalised using Mica-Mg-NP (with Rb-Sr values acquired via MC-ICP-MS) over two measurement sessions.

Figure S13. Isochron diagrams and calculated *in situ* Rb-Sr ages of GL-O grains (natural glauconite). Data were acquired by LA-ICP-MS/MS and normalised using GL-O-NP (with assumed age of 99.6 Ma) over three measurement sessions.

Figure S14. Isochron diagrams and calculated *in situ* Rb-Sr ages of MDC (natural phlogopite). Data were acquired by LA-ICP-MS/MS and normalised using GL-O-NP (with assumed age of 99.6 Ma) over three measurement sessions.

Figure S15. Isochron diagrams and calculated *in situ* Rb-Sr ages of Mica-Fe-NP (biotite). Data were acquired by LA-ICP-MS/MS and normalised using GL-O-NP (with assumed age of 99.6 Ma) over two measurement sessions.

Figure S16. Isochron diagrams and calculated *in situ* Rb-Sr ages of GL-O grains (natural glauconite). Data were acquired by LA-ICP-MS/MS and normalised using GL-O-NP (with assumed age of 95.4 Ma) over three measurement sessions.

Figure S17. Isochron diagrams and calculated *in situ* Rb-Sr ages of MDC (natural phlogopite). Data were acquired by LA-ICP-MS/MS and normalised using GL-O-NP (with assumed age of 95 Ma) over three measurement sessions.

Figure S18. Isochron diagrams and calculated *in situ* Rb-Sr ages of Mica-Fe-NP (biotite). Data were acquired by LA-ICP-MS/MS and normalised using GL-O-NP (with assumed age of 95 Ma) over two measurement sessions.

Figure S19. Isochron diagrams and calculated *in situ* Rb-Sr ages of GL-O grains (natural glauconite). Data were acquired by LA-ICP-MS/MS and normalised using GL-O-NP (with assumed age of 90.4 Ma) over three measurement sessions.

Figure S20. Isochron diagrams and calculated *in situ* Rb-Sr ages of MDC (natural phlogopite). Data were acquired by LA-ICP-MS/MS and normalised using GL-O-NP (with values acquired via MC-ICP-MS) over three measurement sessions.

Figure S21. Isochron diagrams and calculated *in situ* Rb-Sr ages of Mica-Fe-NP (biotite). Data were acquired by LA-ICP-MS/MS and normalised using GL-O-NP (with Rb-Sr values acquired via MC-ICP-MS) over two measurement sessions.

Appendix S1.

Table S1. Measurement results for Rb and Sr mass fractions in pressed nano-powder pellets and glasses determined by LA-ICP-MS/MS.

Table S2. $^{87}Rb/^{86}Sr$ and $^{87}Sr/^{86}Sr$ ratio measurement results for each reference material.

Table S3. Rubidium and Sr mass fraction, and $^{87}Rb/^{86}Sr$ and $^{87}Sr/^{86}Sr$ isotope ratio measurement results for reference materials Mica-Mg and GL-O RMs by isotope dilution MC-ICP-MS.

Table S4. Measurement results for Mica-Mg-NP by LA-ICP MS/MS. Test portions were analysed over two or three measurement sessions.

Table S5. Measurement results for test portions of GL-O-NP analysed over two or three sessions.

Table S6. Details of reference materials (samples, age, standard deviation, measurement session and accuracy).

This material is available from: http://onlinelibrary.wiley.com/doi/10.1111/ggr.12467/abstract (This link will take you to the article abstract).